



CERN-EP-2018-315
20 November 2018

Charged-particle pseudorapidity density at mid-rapidity in p–Pb collisions at $\sqrt{s_{\text{NN}}} = 8.16$ TeV

ALICE Collaboration*

Abstract

The pseudorapidity density of charged particles, $dN_{\text{ch}}/d\eta$, in p–Pb collisions has been measured at a centre-of-mass energy per nucleon-nucleon pair of $\sqrt{s_{\text{NN}}} = 8.16$ TeV at mid-pseudorapidity for non-single-diffractive events. The results cover 3.6 units of pseudorapidity, $|\eta| < 1.8$. The $dN_{\text{ch}}/d\eta$ value is 19.1 ± 0.7 at $|\eta| < 0.5$. This quantity divided by $\langle N_{\text{part}} \rangle / 2$, is 4.73 ± 0.20 , which is 9.5% higher than the corresponding value for p–Pb collisions at $\sqrt{s_{\text{NN}}} = 5.02$ TeV. Measurements are compared with models based on different mechanisms for particle production. All models agree within uncertainties with data in the Pb-going side, while HIJING overestimates, showing a symmetric behaviour, and EPOS underestimates the p-going side of the $dN_{\text{ch}}/d\eta$ distribution. Saturation-based models reproduce the distributions well for $\eta > -1.3$. The $dN_{\text{ch}}/d\eta$ is also measured for different centrality estimators, based both on the charged-particle multiplicity and on the energy deposited in the Zero-Degree Calorimeters. A study of the implications of the large multiplicity fluctuations due to the small number of participants for systems like p–Pb in the centrality calculation for multiplicity-based estimators is discussed, demonstrating the advantages of determining the centrality with energy deposited near beam rapidity.

arXiv:1812.01312v1 [nucl-ex] 4 Dec 2018

© 2018 CERN for the benefit of the ALICE Collaboration.

Reproduction of this article or parts of it is allowed as specified in the CC-BY-4.0 license.

*See Appendix A for the list of collaboration members

1 Introduction

Particle production in proton–nucleus (pA) collisions is influenced by nuclear effects in the initial state. In particular, p–Pb collisions are a valuable tool to study initial-state effects, which are present as a consequence of the nucleons being bound into nuclei. Additionally, the particle multiplicity is an important tool to study the various theoretical models of gluon saturation, which contain different treatments of the upper limit in the growth of the parton density. Therefore, pseudorapidity density measurements can provide constraints to the modelling of the initial state at small Bjorken- x . Moreover, evidence for collective phenomena have been observed in p–Pb collisions, with the magnitude of the effects increasing with event multiplicity [1–9]. Proton–nucleus collisions serve as a tool to study also final-state effects that are sensitive to the formation of a Quark–Gluon Plasma in heavy-ion collisions, under active scrutiny by the community [10]. For these reasons, it is important to understand the collision geometry and the global properties of the system produced in p–Pb collisions.

This paper presents a measurement of the primary charged-particle density in p–Pb collisions, $dN_{\text{ch}}/d\eta_{\text{lab}}$, at a nucleon-nucleon centre-of-mass energy of $\sqrt{s_{\text{NN}}} = 8.16$ TeV for laboratory pseudorapidities $|\eta_{\text{lab}}| < 1.8$. A primary charged particle is defined as a charged particle with a mean proper lifetime τ larger than $1 \text{ cm}/c$, which is either produced directly in the interaction, or from decays of particles with τ smaller than $1 \text{ cm}/c$, excluding particles produced in interactions with the beam pipe, material of the subdetectors, cables and support structures [11]. The dominant processes in p–Pb collisions are the non-diffractive ones. Diffractive events can be single-, double- or central-diffractive and results are presented for non-single-diffractive (NSD) events. Data are compared to other experimental measurements available in pp, p–Pb, d–Au and AA collisions. Results are compared also with simulations (performed with HIJING 2.1 [12, 13], EPOS 3 [14–16] and EPOS LHC [17]) and calculations incorporating the saturation of the gluon density in the colliding hadrons (MC-rcBK [18, 19] and KLN [20, 21]).

The rest of this article is organised in the following way: Sec. 2 describes the experimental conditions and the detectors used to measure the centrality of the event and the pseudorapidity density of charged particles. In Sec. 3, the centrality determination methodologies are described, both the ones using the multiplicity distributions of charged particles and the alternative one that relies on the energy collected in the neutron Zero-Degree Calorimeters (ZDCs). Section 4 explains, in detail, the analysis procedure to measure the $dN_{\text{ch}}/d\eta$. The systematic uncertainties are described in Sec. 5, and the results along with comparisons to models are presented in Sec. 6. A brief summary and conclusions are given in Sec. 7.

2 Experimental setup

The p–Pb data were provided by the Large Hadron Collider (LHC) in December 2016. There were two configurations that were exploited: in one, denoted by p–Pb below, the proton beam circulated towards the negative z direction in the ALICE laboratory system, while ^{208}Pb ions circulated in the opposite direction; in the second configuration, denoted by Pb–p, the direction of both beams was reversed. The total luminosity was 0.06 nb^{-1} , corresponding to around 120 million minimum-bias (MB) events in the p–Pb and Pb–p configurations. The beams in both rings have the same magnetic rigidity. The nucleon-nucleon centre-of-mass energy was $\sqrt{s_{\text{NN}}} = 8.16$ TeV, with both p and Pb beams at 6.5 TeV per proton charge. Due to the asymmetric collision system, there is a shift in the centre-of-mass rapidity of $\Delta y = 0.465$ in the direction of the proton beam.

Full details of the ALICE detector are given elsewhere [22, 23]. The main element used for the analysis was the Silicon Pixel Detector (SPD): the two innermost cylindrical layers of the ALICE Inner Tracking System [22], made of hybrid silicon pixel chips. The SPD is located inside a solenoidal magnet that provides a magnetic field of 0.5 T. The first layer covers $|\eta_{\text{lab}}| < 2.0$ for collisions at the nominal Interaction Point (IP), while the second covers $|\eta_{\text{lab}}| < 1.4$. The layers have full azimuthal coverage and radii of 3.9 cm and 7.6 cm, respectively. In total, the SPD has 9.8×10^6 silicon pixels, each of size $50 \times 425 \mu\text{m}^2$.

The MB trigger signal is given by the V0 detector [24], which is composed of two arrays of 32 scintillators positioned at 3.3 m (V0A) and -0.90 m (V0C) from the nominal IP along the beam axis. Each array has a ring structure segmented into 4 radial and 8 azimuthal sectors. The detector has full azimuthal coverage in the pseudorapidity ranges $2.8 < \eta_{\text{lab}} < 5.1$ and $-3.7 < \eta_{\text{lab}} < -1.7$. The signal amplitudes and particle arrival times are recorded for each of the 64 scintillators. The V0 is well suited for triggering thanks to its good timing resolution (below 1 ns) and its large angular acceptance. The timing is used to discriminate the beam–beam collisions from background events, like beam–gas and beam–halo events, produced outside the interaction region. The neutron ZDCs [25] are likewise utilised for background rejection. The neutron calorimeters, ZNs, are quartz-fibre spaghetti calorimeters placed at zero degrees with respect to the LHC beam axis, positioned at 112.5 m (ZNA) and -112.5 m (ZNC) from the nominal IP. ZNs detect neutral particles emitted at pseudorapidities $|\eta_{\text{lab}}| > 8.7$ and have an energy resolution of around 18% for neutron energies of 2.56 TeV.

A subsample of 6.8 million events is analysed for p–Pb collisions, with an average number of interactions per bunch crossing, $\langle \mu \rangle$ of 0.004. A subsample of 2.7 million events is analysed for Pb–p collisions, with $\langle \mu \rangle = 0.007$. The comparison of p–Pb and Pb–p results is used to assess the systematic uncertainties. The hardware MB trigger is configured to have high efficiency for hadronic events, requiring a signal in both V0A and V0C. Beam–gas and beam–halo interactions are suppressed in the analysis by requiring offline the particles' arrival time in the V0 and ZN detectors to be compatible with collisions from the nominal IP. The contamination from background is estimated to be negligible through control triggers on non-colliding bunches.

The event sample after trigger and timing selection consisted of NSD, single-diffractive (SD), and electromagnetic (EM) interactions. The MB trigger efficiency for NSD events is estimated to be 99.2% using the DPMJet Monte Carlo event generator [26], and 99.5% using HIJING 1.36 [27]. HIJING 1.36 combines perturbative-QCD processes with soft interactions, and includes a strong impact parameter dependence of parton shadowing. DPMJet is based on the Gribov-Glauber approach and treats soft and hard scattering processes in a unified way. It includes incoherent SD collisions of the projectile proton with target nucleons; these interactions are concentrated mainly on the surface of the nucleus. The generated particles are transported through the experimental setup using the GEANT3 [28] software package. SD collisions are removed in DPMJet by requiring that at least one of the binary nucleon-nucleon interactions is NSD. The SD and EM contaminations are estimated from Monte Carlo simulation studies to be negligible.

Among the selected events in data, 99% had a primary vertex. In DPMJet this fraction was 99.6% (99.8% for HIJING 1.36), with a trigger and selection efficiency for events without a primary vertex of 28% (23.1%). Taking into account the difference of the fraction of events without a vertex in the data and the simulation, the overall selection efficiency for NSD events in the analysis is estimated to be 97.0% (96.2%) according to DPMJet (HIJING 1.36).

3 Centrality determination

The Glauber model [29, 30] is used to calculate the number of participating nucleons (participants), N_{part} , and the corresponding number of nucleon-nucleon collisions, N_{coll} , that are controlled by the collision impact parameter, b . Indeed, the number of produced particles changes with the variation of the amount of matter overlapping in the collision region; N_{part} and N_{coll} describe quantitatively this variation. In pA collisions, $N_{\text{coll}} = N_{\text{part}} - 1$. Using the Glauber model, it is possible to calculate the probability distributions of the relevant parameters, N_{part} and N_{coll} , which for pA collisions are loosely correlated to b . Centrality classes are defined as percentile intervals of the visible cross section, which determines the event sample after the selections described in Sec. 2. The number of participating nucleons and nucleon-nucleon collisions are calculated, accordingly, for the visible cross section.

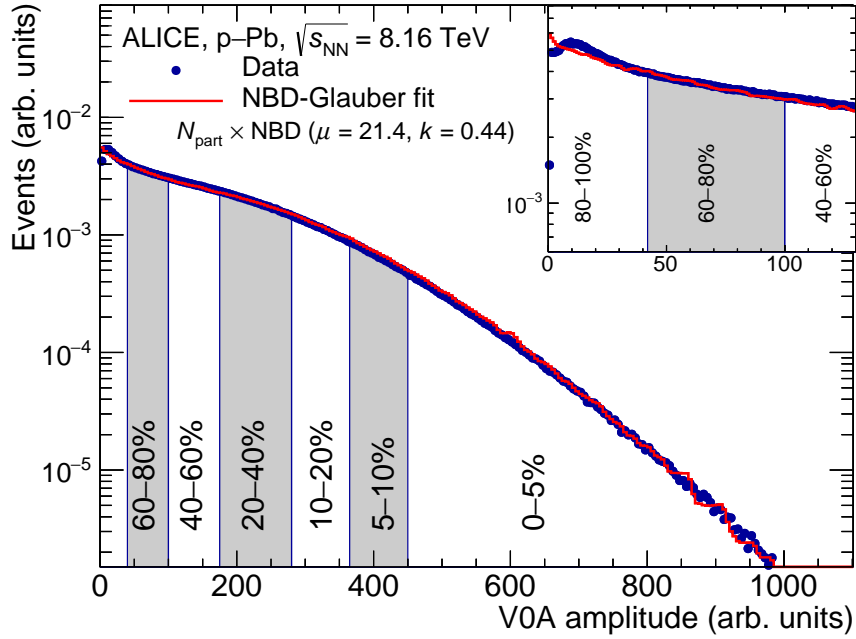


Figure 1: Distribution of the sum of amplitudes in V0A (Pb-going side) and the NBD-Glauber fit in red. Centrality classes are indicated by vertical lines and the inset shows the most peripheral events in more detail.

The centrality is determined for three different estimators, two of which are based on observables well separated in pseudorapidity to limit the effect of short-range correlations in the collision region. The method founded on multiplicity-based estimators is derived by fitting the measured charged-particle multiplicity distributions with an N_{coll} distribution obtained from the Glauber model convoluted with a Negative Binomial Distribution (NBD) to model the multiplicity produced in a single collision. Multiplicity fluctuations play an important role in pA collisions. The range of multiplicities used to define a centrality class in the case of pA collisions is of the same order of magnitude as the multiplicity fluctuations [31]. Therefore, a biased sample of nucleon-nucleon collisions is selected using multiplicity. Samples of high-multiplicity events select not only a class with larger than average $\langle N_{part} \rangle$, but also one which is widely spread in N_{coll} and that leads to deviations from the scaling of hard processes with Multiple Parton Interactions (MPI). These high-multiplicity nucleon-nucleon collisions have a higher particle mean transverse momentum p_T , and are collisions where MPI are more likely [4]. The opposite happens for low-multiplicity events.

The centrality determined from the hybrid method, described in Sec. 3.2 using the energy deposited in the ZDCs, on the contrary, minimises biases on the binary scaling of hard processes. Indeed, the ZDCs detect, at large η separation from the central region, the nucleons produced in the interaction through the nuclear de-excitation process or knocked out by participants (called slow nucleons). A heuristic approach based on extrapolation from low-energy data is discussed in a previous publication [31].

3.1 Centrality from charged-particle distributions

In the method based on multiplicity estimators [31], the events are classified into centrality classes using either the number of clusters in the outer layer of the SPD (CL1 estimator), or the amplitude measured by the V0 in the Pb-remnant side, A-side, for p-Pb (V0A estimator) or in the C-side for Pb-p (V0C estimator) collisions. The amplitudes are fitted with a Monte Carlo implementation of the Glauber model assuming that the number of sources is given by the $N_{part}/2$ multiplied by a NBD, which is the assumed particle production per source, parametrised with μ and k , where μ is the mean multiplicity per source and k controls the contribution at high multiplicity. The nuclear density for Pb is modelled by

Table 1: Mean values of N_{part} , N_{coll} and T_{pPb} of p–Pb collisions for MB and centrality classes defined by slices in CL1 and V0A. The values are obtained with a Glauber Monte Carlo calculation coupled to an NBD to fit CL1 and V0A distributions.

| Centrality (%) | $\langle N_{\text{part}} \rangle$ | RMS | syst. | $\langle N_{\text{coll}} \rangle$ | RMS | syst. | $\langle T_{\text{pPb}} \rangle$ (mb $^{-1}$) | RMS (mb $^{-1}$) | syst. (mb $^{-1}$) |
|----------------|-----------------------------------|-----|-------|-----------------------------------|-----|-------|--|-------------------|---------------------|
| 0–100 | 8.09 | 5.3 | 0.17 | 7.09 | 5.3 | 0.16 | 0.0978 | 0.073 | 0.0021 |
| CL1 Estimator | | | | | | | | | |
| 0–5 | 17.0 | 3.6 | 0.6 | 16.0 | 3.6 | 0.6 | 0.220 | 0.050 | 0.008 |
| 5–10 | 15.0 | 3.5 | 0.4 | 14.0 | 3.5 | 0.4 | 0.193 | 0.048 | 0.006 |
| 10–20 | 13.4 | 3.5 | 0.4 | 12.4 | 3.5 | 0.4 | 0.172 | 0.048 | 0.004 |
| 20–40 | 10.9 | 3.6 | 0.2 | 9.9 | 3.6 | 0.2 | 0.136 | 0.050 | 0.003 |
| 40–60 | 7.47 | 3.3 | 0.15 | 6.47 | 3.3 | 0.15 | 0.0893 | 0.046 | 0.0022 |
| 60–80 | 4.53 | 2.4 | 0.09 | 3.53 | 2.4 | 0.09 | 0.0487 | 0.033 | 0.0013 |
| 80–100 | 2.76 | 1.2 | 0.03 | 1.76 | 1.2 | 0.03 | 0.0242 | 0.016 | 0.0004 |
| V0A Estimator | | | | | | | | | |
| 0–5 | 16.5 | 3.8 | 0.6 | 15.5 | 3.8 | 0.6 | 0.213 | 0.052 | 0.008 |
| 5–10 | 14.6 | 3.7 | 0.4 | 13.6 | 3.7 | 0.4 | 0.188 | 0.052 | 0.006 |
| 10–20 | 13.1 | 3.9 | 0.4 | 12.1 | 3.9 | 0.4 | 0.167 | 0.053 | 0.004 |
| 20–40 | 10.7 | 4.0 | 0.2 | 9.7 | 4.0 | 0.2 | 0.134 | 0.055 | 0.003 |
| 40–60 | 7.64 | 3.7 | 0.16 | 6.64 | 3.7 | 0.16 | 0.0916 | 0.051 | 0.0023 |
| 60–80 | 4.80 | 2.7 | 0.10 | 3.80 | 2.7 | 0.10 | 0.0525 | 0.037 | 0.0013 |
| 80–100 | 2.88 | 1.4 | 0.03 | 1.88 | 1.4 | 0.03 | 0.0260 | 0.019 | 0.0004 |

a Woods-Saxon distribution for a spherical nucleus with a radius of 6.62 ± 0.06 fm and a skin thickness of 0.55 ± 0.01 fm [32]. The hard-sphere exclusion distance between nucleons is 0.40 ± 0.40 fm. For $\sqrt{s_{\text{NN}}} = 8.16$ TeV collisions, an inelastic nucleon-nucleon cross section of 72.5 ± 0.5 mb is used, obtained by interpolation of cross section experimental values [32].

The measured V0A distribution with the NBD-Glauber fit is shown in Fig. 1. A similar fit has been performed for the CL1 estimator. The failure of the chosen fit function for amplitudes smaller than about 10 is due to trigger inefficiencies in peripheral collisions. The average number of participants, collisions and nuclear overlap function, $\langle T_{\text{pPb}} \rangle$, are calculated from the NBD-Glauber simulation for every defined centrality class. The values for the different estimators are given in Tab. 1. The systematic uncertainties are obtained by repeating the fit, varying the Glauber parameters (radius, skin thickness and hard-sphere exclusion) within their uncertainties. The number of participants for all selected events is on average $N_{\text{part}} = 8.09 \pm 0.17$. The increase in the average N_{part} , when calculated for NSD collisions only, is of around 2% and within systematic uncertainties. The geometrical properties determined with the NBD-Glauber model are robust and approximately independent of the centrality estimator used, within the model assumptions of this approach.

3.2 Centrality from Zero-Degree Calorimeter and the hybrid method

The ZN detect the slow neutrons produced in the interaction. The multiplicity of slow nucleons is monotonically related to N_{coll} , and can, therefore, be used to determine the centrality of the collision [31]. The experimental distribution of the ZN energy is shown in Fig. 2 and it is used for the hybrid method, which aims to provide an unbiased centrality estimator. It is based on two assumptions, the first is that the event selection based on the energy deposited in the ZDCs is free from the multiplicity fluctuation biases in the particle production at mid-rapidity. The second assumption is that the wounded nucleon model holds [33] and that some observables, defined below, scale linearly with N_{coll} and N_{part} allowing one to establish a relationship to the collision geometry. Two sets of $\langle N_{\text{coll}} \rangle$ are calculated: $N_{\text{coll}}^{\text{mult}}$ and $N_{\text{coll}}^{\text{Pb-side}}$ for each centrality bin i estimated using ZN. The first set is computed assuming that the charged-particle multiplicity at mid-rapidity is proportional to the N_{part} : $\langle N_{\text{part}} \rangle_i^{\text{mult}} = \langle N_{\text{part}} \rangle_{\text{MB}} \cdot (\langle dN_{\text{ch}}/d\eta_{\text{lab}} \rangle_i / \langle dN_{\text{ch}}/d\eta_{\text{lab}} \rangle_{\text{MB}})$, where $\langle N_{\text{part}} \rangle_{\text{MB}}$ is the average number of participating nucleons in MB collisions reported in Tab. 1, and, consequently: $\langle N_{\text{coll}} \rangle_i^{\text{mult}} = \langle N_{\text{part}} \rangle_i^{\text{mult}} - 1$. The second set is calculated using the Pb-side multiplic-

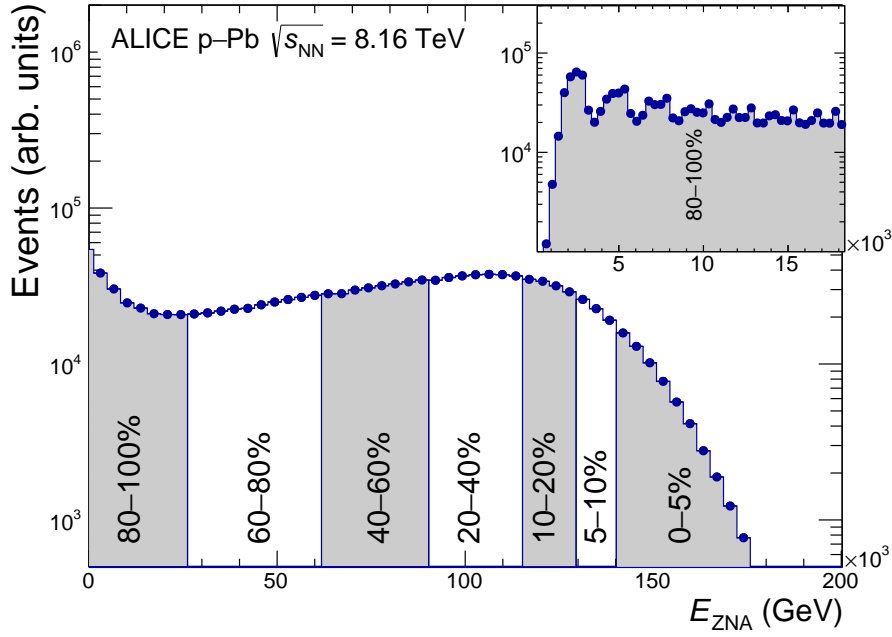


Figure 2: Distribution of the neutron energy spectrum measured in the Pb-going side (ZNA). Centrality classes are indicated by vertical lines and the inset shows the most peripheral events in more detail.

Table 2: Average number of hadronic nucleon collisions for the ZNA estimator, with the assumption of charged-particle multiplicity at mid-rapidity proportional to N_{part} , $\langle N_{\text{coll}} \rangle^{\text{mult}}$, and assuming the signal in V0 proportional to N_{coll} , $\langle N_{\text{coll}} \rangle^{\text{Pb-side}}$.

| Centrality (%) | $\langle N_{\text{coll}} \rangle^{\text{mult}}$ | $\langle N_{\text{coll}} \rangle^{\text{Pb-side}}$ | syst. (%) |
|----------------|---|--|-----------|
| 0–5 | 13.4 | 14.2 | 6.4 |
| 5–10 | 12.5 | 12.9 | 3.9 |
| 10–20 | 11.5 | 11.8 | 3.4 |
| 20–40 | 9.81 | 9.77 | 2.3 |
| 40–60 | 7.09 | 6.83 | 4.3 |
| 60–80 | 4.28 | 4.09 | 4.9 |
| 80–100 | 2.08 | 2.13 | 3.3 |

ity: $\langle N_{\text{coll}} \rangle_i^{\text{Pb-side}} = \langle N_{\text{coll}} \rangle_{\text{MB}} \cdot (\langle S \rangle_i / \langle S \rangle_{\text{MB}})$, where S is the raw signal of the innermost ring of V0A for p-Pb ($4.5 < \eta_{\text{lab}} < 5.1$) and V0C for Pb-p collisions ($-3.7 < \eta_{\text{lab}} < -3.2$). A comparison of the N_{coll} values obtained for the various estimators is reported in Tab. 2 for p-Pb collisions. The two different sets are consistent among each other and with the values calculated for Pb-p. The systematic uncertainties come from the uncertainty on the N_{coll} for 0–100% in Tab. 1 summed with the maximum difference between the $N_{\text{coll}}^{\text{mult}}$ and $N_{\text{coll}}^{\text{Pb-side}}$.

4 Analysis procedure

The technique for the $dN_{\text{ch}}/d\eta_{\text{lab}}$ measurement is the same as the one employed at $\sqrt{s_{\text{NN}}} = 5.02$ TeV [31, 34]. The pseudorapidity acceptance in the laboratory system depends on the position of the primary vertex along the beamline, z_{vtx} . The selection of a reconstructed vertex within $|z_{\text{vtx}}| < 15$ cm allows a range of $|\eta_{\text{lab}}| < 1.8$ to be covered. Tracklet candidates (short track segments) are formed using the position of the primary vertex and two hits in the SPD, one in the first and one in the second layer. Tracklets produced by the random combination of two hits are rejected. To do so, the angular difference

Table 3: Overview of the sources of systematic uncertainties.

| Source | Uncertainty (%) | | | | | |
|------------------------------------|-----------------|----------------|------------|----------------|------------|----------------|
| | 0–100% | | 0–5% | | 80–100% | |
| | $\eta = 0$ | $ \eta = 1.8$ | $\eta = 0$ | $ \eta = 1.8$ | $\eta = 0$ | $ \eta = 1.8$ |
| Tracklet selection criteria | negligible | 0.5 | negligible | 0.5 | negligible | 0.5 |
| Weak-decay contamination | 1.3 | | 1.3 | | 1.3 | |
| Detector acceptance and efficiency | 2.2 | | 2.2 | | 2.2 | 2.8 |
| Trigger efficiency | 0.8 | | – | | 1.7 | |
| Event-generator dependence | 1.2 | | – | | – | |
| Background subtraction | 0.3 | | 0.3 | | 0.3 | |
| Material budget | 0.1 | | 0.1 | | 0.1 | |
| Particle composition | 0.3 | | 0.3 | | 0.3 | |
| Zero- p_{T} extrapolation | negligible | | negligible | | negligible | |
| Pileup | negligible | | negligible | | negligible | |
| Total | 3.0 | | 2.6 | | 3.1 | 3.6 |

in the azimuthal direction, $\Delta\phi$, and in the polar direction, $\Delta\theta$, of the inner and outer layer hit with respect to the reconstructed primary vertex is determined for each pair of hits. Afterwards, the sum of the squares of the weighted differences in azimuth and polar angles $\delta^2 = (\Delta\phi/\sigma_\phi)^2 + (\Delta\theta/\sigma_\theta)^2$ is required to be less than 1.5, where $\sigma_\phi = 60$ mrad and $\sigma_\theta = 25 \sin^2 \theta$ mrad. With such a requirement, tracklets corresponding to charged particles with $p_{\text{T}} > 50$ MeV/ c are effectively selected. Particles with lower p_{T} are mostly absorbed by the detector material or lost due to the bending in the magnetic field.

The raw multiplicity measured by tracklets needs to be corrected for (i) the probability for a primary particle to be reconstructed as a tracklet (acceptance and efficiency), (ii) the contribution from combinatorial tracklets, i.e. those whose two hits do not originate from the same primary particle, (iii) the difference between the fraction of events without a vertex in the data and in the simulation and (iv) the secondary-particle contamination. The first three corrections are computed using simulated data from the HIJING 1.36 or DPMJet event generators. The centrality definition in the simulated data is adjusted such that the particle density is similar to that in real data for the same centrality classes. The contributions (i) and (ii), determined as a function of z and η_{lab} , are on average around 1.5 for the acceptance and reconstruction efficiency, and around 0.02 for the combinatorial background removal in MB and centrality-dependent measurements at mid-rapidity, independently of the estimator selected and the centrality class. At $|\eta_{\text{lab}}| = 1.8$ the combinatorial background contribution reaches a maximum value of 0.07. We further correct the measurement by the difference in the fraction of events without a vertex observed in data and simulation. The correction for MB $dN_{\text{ch}}/d\eta_{\text{lab}}$ amounts to 2.2% (3.4%) when using DPMJet (HIJING 1.36). Since the centrality classes are defined as percentiles of the visible cross section, the centrality-dependent measurements are not corrected for the trigger inefficiencies. Differences in strange-particle content observed at lower beam energies [6, 35] have been used for a data-driven correction applied to the generator output, giving rise to a correction factor of -0.6% , independent of centrality.

5 Systematic uncertainties

Several sources of systematic uncertainties were investigated. The uncertainty coming from the selection of the tracklet quality value δ^2 is negligible at mid-rapidity and amounts to 0.5% at $|\eta_{\text{lab}}| = 1.8$. The other uncertainties associated to the MB $dN_{\text{ch}}/d\eta_{\text{lab}}$ are independent of the pseudorapidity. The uncertainty resulting from the subtraction of the contamination from weak decays of strange hadrons is estimated to be about 1.3%. It is estimated by varying the amount of strange particles except kaons by $\pm 50\%$. The uncertainty in detector acceptance and reconstruction efficiency is estimated to be 2.2% by carrying out the analysis for different slices of the z_{vtx} position distribution and with subsamples in azimuth. The measurement for Pb–p collisions gives rise to an additional contribution of 1.8%, when reflected in η_{lab} ,

for the most peripheral centrality bins (80–100%), and 1.1% for 60–80% at $|\eta_{\text{lab}}| = 1.8$, and is added to the systematic uncertainty for acceptance. For the other centrality bins and the MB result the difference among p–Pb and Pb–p is negligible and already accounted for in the acceptance and reconstruction efficiency uncertainty. The uncertainty related to the trigger and event selection efficiency for NSD collisions is estimated to be 0.8% by taking into account the differences in the efficiency obtained with HIJING 1.36 and DPMJet. An additional 1.2% uncertainty comes from the difference in the scaling factors due to the events without vertex using the two event generators, as discussed in Sec. 4. A Monte Carlo test was also carried out with DPMJet to check the difference in the results obtained from NSD generated events and from selected events, resulting in a difference of 0.2% for the MB result, absorbed in the trigger efficiency uncertainty, and of 1.7% (0.2%) for 80–100% (60–80%) centrality bins. The contribution due to the subtraction of the background is studied using an alternative method where fake hits are injected into real events and it gives rise to a 0.3% uncertainty. The uncertainty from the material budget is 0.1%, while the uncertainty due to the particle composition amounts to 0.3%. The contributions from the extrapolation down to zero p_{T} and from the pileup are found to be negligible.

The final systematic uncertainties assigned to the measurements are the quadratic sums of the individual contributions. An overview of the systematic uncertainties is presented in Tab. 3. For MB $dN_{\text{ch}}/d\eta_{\text{lab}}$, they amount to 3.0%. For centrality-dependent measurements the total uncertainty for central events is 2.6%. For the most peripheral events it is 3.1% at mid-rapidity and 3.6% for $|\eta_{\text{lab}}| = 1.8$. The difference in uncertainty between the MB and the centrality-dependent measurement is mostly due to the contributions from the selection efficiency for NSD, which are not included in the centrality-dependent measurement, and to the difference among p–Pb and Pb–p collisions, which is more relevant for the most peripheral events at $|\eta_{\text{lab}}| = 1.8$.

6 Results

The pseudorapidity density as a function of η_{lab} is presented in Fig. 3 for $|\eta_{\text{lab}}| < 1.8$. An asymmetry between the proton and the lead hemispheres is observed, and the number of charged particles is higher in the Pb-going side (positive η_{lab}). The ALICE measurement is compared with the pseudorapidity density measured by CMS [36] showing very good agreement within systematic uncertainties. The result is also compared with several models with different descriptions of particle production, all shifted by $\eta_{\text{lab}} = 0.465$ to take into account the shift to the laboratory system. In the improved HIJING 2.1 [12, 13] version the Cronin effect is included, as well as a strong nuclear shadowing effect ($sg = 0.28$) in order to explain the global properties of the final hadron system in p–Pb collisions [34]. The model describes well both the normalisation and the shape of the distribution for the Pb-going side, while it overestimates the p-going side, showing a symmetric behaviour, as for the p–Pb collisions at 5.02 TeV. The $dN_{\text{ch}}/d\eta_{\text{lab}}$ versus η_{lab} is compared with two different versions of EPOS. EPOS LHC [17] is a tune of EPOS 1.99 based on LHC data. It is designed to describe all bulk properties of hadronic interactions and based on Gribov-Regge theory for partons. It incorporates collective effects with a separation of the initial state into a core and a corona. EPOS LHC reproduces the Pb-going side, although it underestimates the p-going side of the distribution, showing a stronger asymmetry than data. EPOS 1.99 contains collective flow parametrised at freeze-out, while EPOS 3 [14–16] includes a full viscous hydrodynamical simulation. It starts from flux tube initial conditions, which are generated in the Gribov-Regge multiple scattering framework. It reproduces the most forward part of the distribution in the Pb-going side, but underestimates both the normalisation, the mid-rapidity part and the p-going side of the $dN_{\text{ch}}/d\eta_{\text{lab}}$ distribution. Finally, the distribution is compared with two saturation-based models: MC-rcBK [18, 19] and KLN [20, 21], which contain a mechanism to limit the number of partons and particles produced. The MC-rcBK results are obtained using the McLerran-Venugopalan model ($\gamma = 1$) [52] for the Albacete-Armesto-Milhano-Quiroga-Salgado initial conditions [53]. Saturation-based models are the ones which perform better. Indeed, both MC-rcBK and KLN reproduce the distribution well, within the uncertainties of data, and

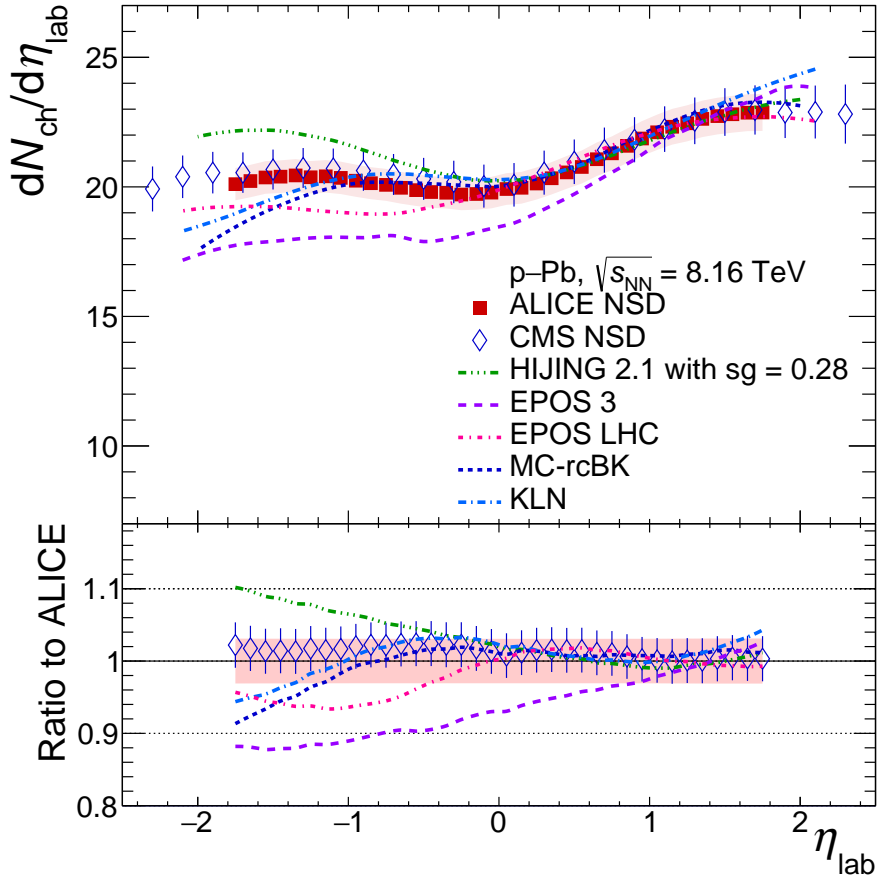


Figure 3: Red squares show the measured pseudorapidity density of charged particles in p–Pb NSD collisions at $\sqrt{s_{\text{NN}}} = 8.16$ TeV in ALICE, with total systematic uncertainties shown as bands, compared with CMS results [36] and theoretical predictions shifted to the laboratory system [12, 14, 17, 18, 20]. The bottom panel shows the ratio to ALICE data.

start to deviate in the region $\eta_{\text{lab}} < -1.3$. The MC-rcBK model better predicts the p–Pb collisions at 8.16 TeV than the distribution at 5.02 TeV. Nevertheless, all models lie within about 10% when compared with data, and reproduce within systematic uncertainties the Pb-going side.

The charged-particle pseudorapidity density in the laboratory system for $|\eta_{\text{lab}}| < 0.5$ is $dN_{\text{ch}}/d\eta_{\text{lab}} = 20.08 \pm 0.01$ (stat.) ± 0.61 (syst.). In the following, the statistical uncertainty is considered to be negligible. The data are integrated in the range $-0.965 < \eta_{\text{lab}} < 0.035$ and corrected for the effect of the rapidity shift to retrieve the $dN_{\text{ch}}/d\eta$ in the centre-of-mass system. The correction for the pseudorapidity shift is estimated from HIJING 1.36 [27] to be $-3.7\% \pm 1.9\%$. The resulting pseudorapidity density in the centre of mass is $dN_{\text{ch}}/d\eta = 19.1 \pm 0.7$.

The charged-particle production is scaled by $N_{\text{part}}/2$, calculated with a Glauber model as explained in Sec. 3, in order to compare the bulk particle production in different collision systems. The number of participants for MB events is 8.09 ± 0.17 . The value normalised to the number of participants divided by 2 gives $dN_{\text{ch}}/d\eta \times (2/N_{\text{part}}) = 4.73 \pm 0.20$. In Fig. 4, this quantity is compared with lower energy p–Pb measurements by ALICE [34] as well as by CMS [36] and d–Au measurements at RHIC [37], showing that the values overlap with $dN_{\text{ch}}/d\eta$ measurements for inelastic pp collisions [38–40]. The dependence of $\langle dN_{\text{ch}}/d\eta \rangle$ on the centre-of-mass energy can be fitted with a power-law function of the form $\alpha \cdot s^\beta$. This gives an exponent, under the assumption of uncorrelated uncertainties, of $\beta = 0.103 \pm 0.002$. It is a much weaker s -dependence than for AA collisions [41–51], where a value of $\beta = 0.152 \pm$

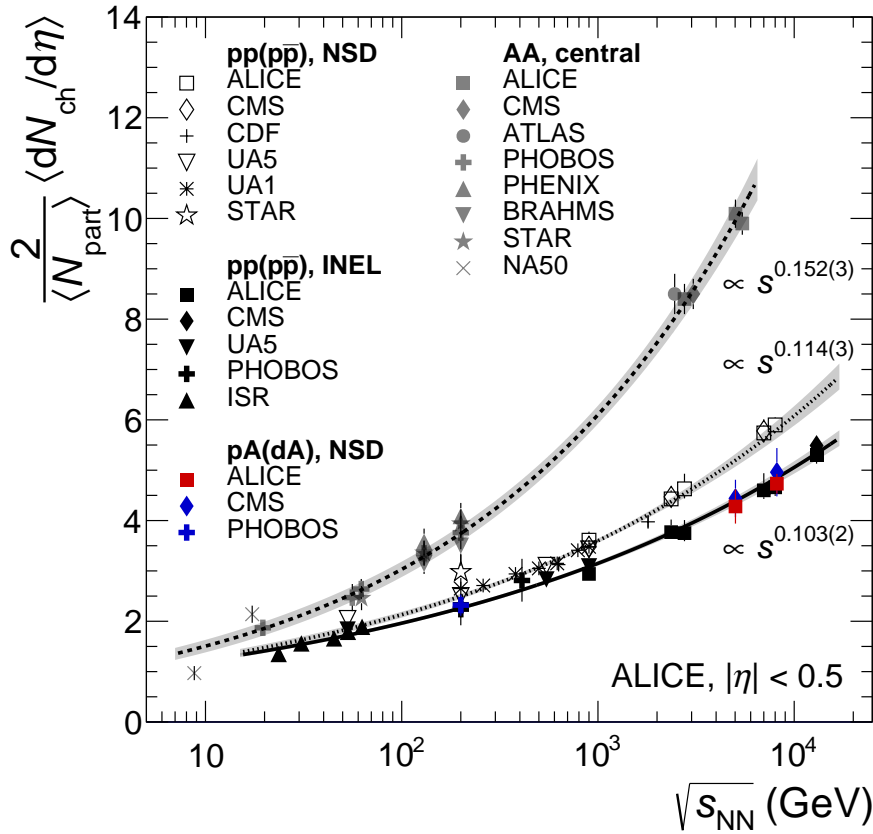


Figure 4: Values of $\frac{2}{\langle N_{part} \rangle} \langle dN_{ch}/d\eta \rangle$ for pA [34, 36, 37], pp and p \bar{p} [38–40] along with those from central AA collisions [41–51] as a function of $\sqrt{s_{NN}}$ are shown, for $|\eta| < 0.5$. All values of $\langle N_{part} \rangle$ used for normalisation of data are the results of Glauber model calculations. The s -dependencies of the pp (p \bar{p}) inelastic (INEL) and p–Pb collisions data are proportional to $s_{NN}^{0.103}$ (solid line), while pp (p \bar{p}) NSD are proportional to $s_{NN}^{0.114}$ (dashed middle line). AA are proportional to $s_{NN}^{0.152}$ (dashed upper line). The bands show the uncertainties on the extracted power-law dependencies.

0.003 is obtained. The fit results are plotted with their uncertainties shown as shaded bands. The result at $\sqrt{s_{NN}} = 8.16$ TeV confirms the trend established by lower energy data since the exponent β is not significantly different when the new point is excluded from the fit. The values for p–Pb and d–Au collisions fall on the inelastic pp curve, indicating that the strong rise in AA might not be solely related to the multiple collisions undergone by the participants since the proton in pA collisions also encounters multiple nucleons. As the contribution of diffractive processes to the selected p–Pb sample is negligible, it is expected that the NSD and inelastic selection belong to the same curve for p–Pb, and that this slope corresponds to the one obtained from the inelastic pp curve.

The pseudorapidity density as a function of η_{lab} is presented in Fig. 5 for $|\eta_{lab}| < 1.8$ for different centrality intervals, from most central 0–5% to most peripheral 80–100% events. The results for the CL1 estimator have a strong bias due to the complete overlap with the tracking region. V0A has a small multiplicity fluctuation bias due to the enhanced contribution from the Pb-fragmentation region. Finally, the ZNA measurement based on the energy deposited in the ZN does not have multiplicity bias. The CL1 (ZNA) estimator produces the largest (lowest) values for the most central events and the lowest (largest) values for the most peripheral events. It is worth noting that for all the estimators used to select centrality the asymmetry is evident for most central events, while the results for 60–80% and 80–100% classes, where the $\langle N_{part} \rangle$ are around 4.5 and 3, respectively, are symmetric.

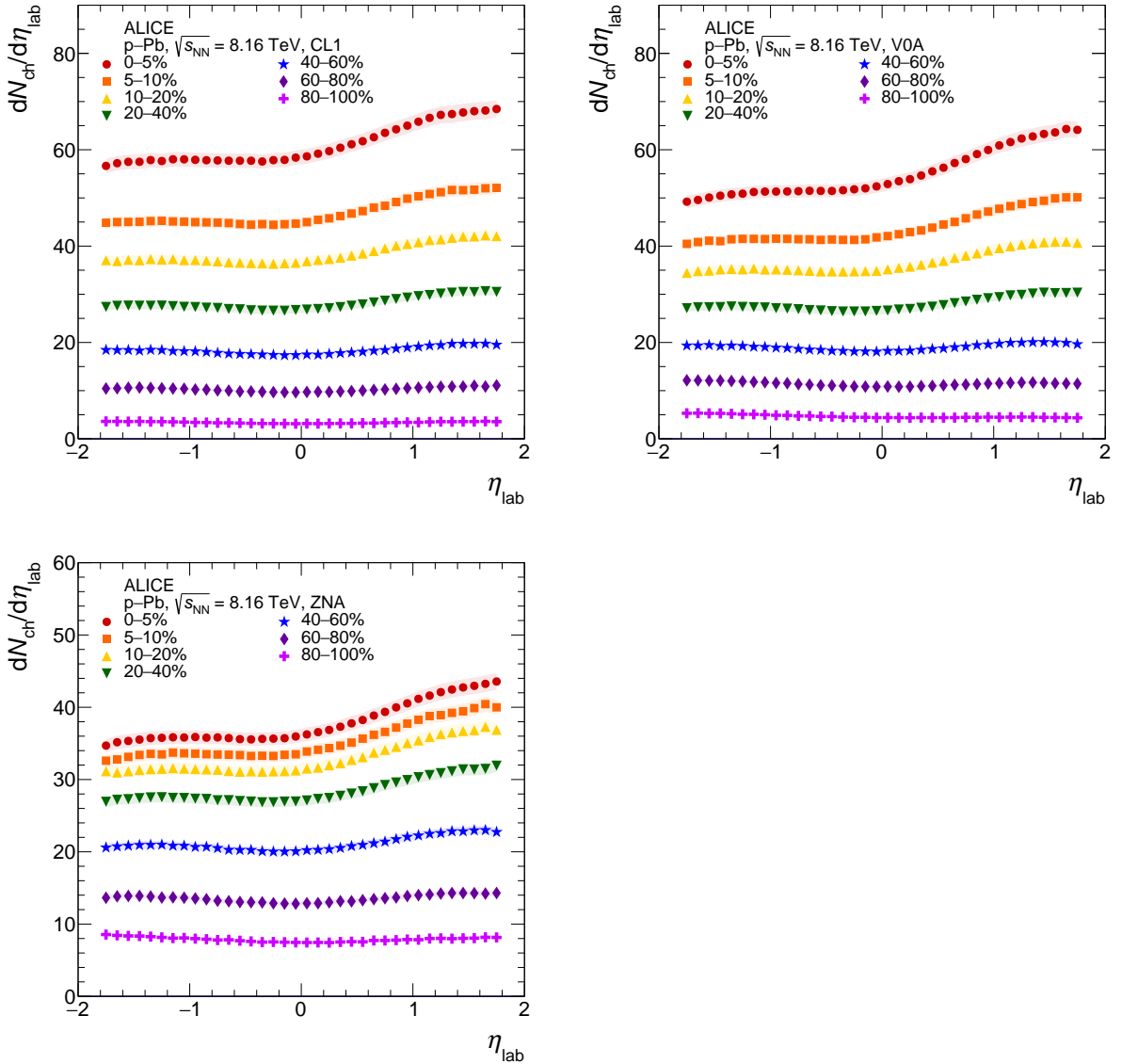


Figure 5: Pseudorapidity density of charged particles in p-Pb NSD collisions at $\sqrt{s_{\text{NN}}} = 8.16$ TeV for various centrality classes and estimators: CL1 (top left), V0A (top right) and ZNA (bottom left).

The left panel of Fig. 6 shows $\frac{2}{\langle N_{\text{part}} \rangle} \langle dN_{\text{ch}}/d\eta_{\text{lab}} \rangle$ as a function of $\langle N_{\text{part}} \rangle$ for various centrality estimators. For CL1 and V0A the $\langle N_{\text{part}} \rangle$ from the Glauber model are used and the resulting $\frac{2}{\langle N_{\text{part}} \rangle} \langle dN_{\text{ch}}/d\eta_{\text{lab}} \rangle$ has a steep increase for most central events (higher $\langle N_{\text{part}} \rangle$) due to the strong multiplicity bias discussed in Sec. 3. The rise is steeper for CL1, where the overlap of the centrality selection region with the tracking region is maximal. For the ZNA estimator, two sets of $\langle N_{\text{part}} \rangle$ are used corresponding to the two different hybrid method selections. For both $N_{\text{part}}^{\text{mult}}$ and $N_{\text{part}}^{\text{Pb-side}}$ the trend is similar and extrapolates to the pp point at $\sqrt{s} = 8$ TeV. The overall $\langle N_{\text{part}} \rangle$ dependence of $\frac{2}{\langle N_{\text{part}} \rangle} \langle dN_{\text{ch}}/d\eta_{\text{lab}} \rangle$ for the ZNA estimator is flat and the $\langle N_{\text{part}} \rangle$ range is more limited when the selection is made in a well separated pseudorapidity region, rather than for multiplicity-based estimators (CL1 and V0A).

A Glauber Monte Carlo calculation based on single quark scattering is also performed [54, 55], as it was done for AA collisions [41, 42]. Quark constituents are located around the nucleon centre, where the proton density is modelled by a function of the proton radius. To account for effective partonic degrees of freedom, $N_c = 5$ quark constituents have been selected. The effective inelastic cross section for

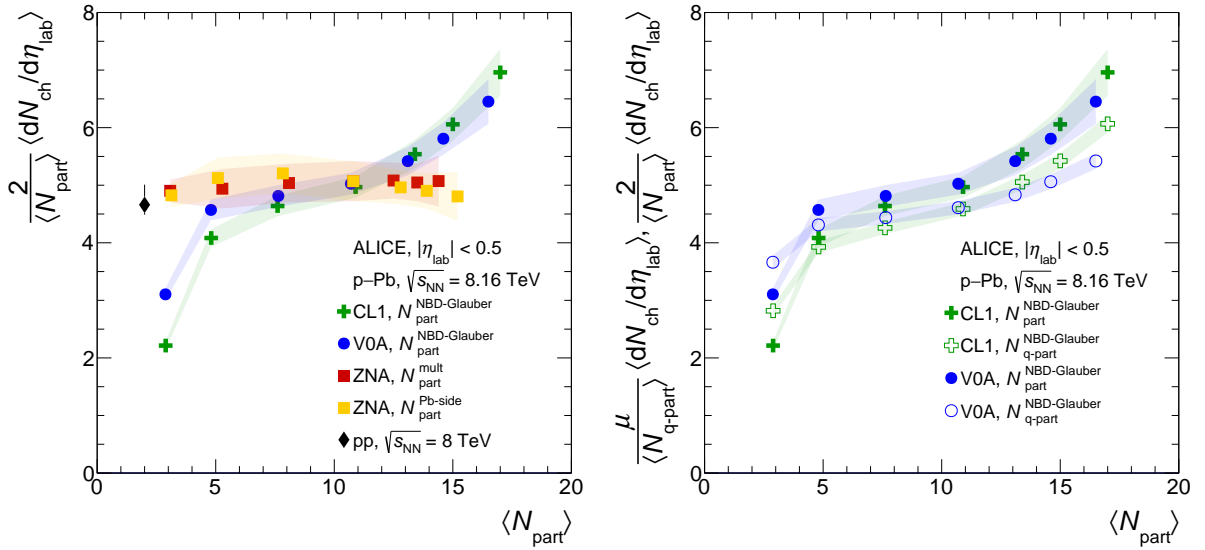


Figure 6: Left: $\frac{2}{\langle N_{\text{part}} \rangle} \langle dN_{\text{ch}}/d\eta_{\text{lab}} \rangle$ in p–Pb collisions at $\sqrt{s_{\text{NN}}} = 8.16$ TeV and pp at 8 TeV [38] as a function of $\langle N_{\text{part}} \rangle$ for different centrality estimators. Right: $\frac{\mu}{\langle N_{\text{q-part}} \rangle} \langle dN_{\text{ch}}/d\eta_{\text{lab}} \rangle$ for $N_c = 5$, open points, with $\mu = 4.44$.

constituent-quark collisions is set to 11.0 mb for 5 constituent quarks to match the 72.5 mb nucleon cross section for p–Pb interactions at 8.16 TeV [30]. The right panel of Fig. 6 shows the $\frac{\mu}{\langle N_{\text{q-part}} \rangle} \langle dN_{\text{ch}}/d\eta_{\text{lab}} \rangle$ scaled by the average number of participating quarks, μ , in pp collisions, which is 4.44 out of 10 participating quarks for $N_c = 5$, as a function of N_{part} (open points). For the multiplicity-based estimators, CL1 and V0A, there is an increase for the most central and decrease for the most peripheral events with a trend that resembles the one for N_{part} scaling (full points) but with decreased slope. This fact suggests that nuclear-geometrical effects are represented in terms of constituent participant quarks, but not as well as observed for AA collisions [41, 42, 56], meaning that the multiplicity-fluctuation bias might influence also the quark participants scaling. The $\frac{\mu}{\langle N_{\text{q-part}} \rangle} \langle dN_{\text{ch}}/d\eta_{\text{lab}} \rangle$ has been measured also for 3 constituent quarks, with an inelastic cross section of 22.5 mb and $\mu = 3.54$, showing a distribution in between the N_{part} and $N_{\text{q-part}}$ points.

7 Summary and conclusions

Summarising, the charged-particle pseudorapidity density in $|\eta_{\text{lab}}| < 1.8$ in NSD p–Pb collisions at $\sqrt{s_{\text{NN}}} = 8.16$ TeV is presented. A value of $dN_{\text{ch}}/d\eta = 19.1 \pm 0.7$ is measured at mid-rapidity, corresponding to 4.73 ± 0.20 charged particles per unit of pseudorapidity per participant pair, $\langle N_{\text{part}} \rangle/2$, calculated with the Glauber model. The new measurement is 9.5% higher than the value at $\sqrt{s_{\text{NN}}} = 5.02$ TeV. The dependence of $\langle dN_{\text{ch}}/d\eta \rangle$ on the centre-of-mass energy is fitted with a power-law function, which gives a much weaker s -dependence than for AA collisions. The MB $dN_{\text{ch}}/d\eta_{\text{lab}}$ distribution as a function of η_{lab} is compared with CMS results, showing good agreement within uncertainties, and to different models: HIJING 2.1, EPOS (versions LHC and 3) and two saturation-based models, MC-rcBK and KLN. All models can reproduce the data within about 10%, which is a sound achievement given the complexity in describing soft-QCD processes. Results provide further constraints for models describing high-energy hadron collisions. The pseudorapidity density for various centrality estimators has been shown and the asymmetry, typical of asymmetric collision systems like p–Pb, is evident for most central events, while results for 60–80% and 80–100% centrality classes are symmetric. The methods to select centrality in p–Pb collisions based on multiplicity measurements have been presented and they induce a multiplicity-fluctuation bias. Results with a selection based on multiplicity estimators at mid-rapidity or

within a few units of pseudorapidity and $\langle N_{\text{part}} \rangle$ from the Glauber model are lower for peripheral values of $\frac{2}{\langle N_{\text{part}} \rangle} \langle dN_{\text{ch}}/d\eta \rangle$ and higher for most central collisions than the pp value. On the contrary, with centrality selected by the energy deposited in the ZDC, and assuming that the multiplicity in the Pb-going direction is proportional to $N_{\text{part}}^{\text{Pb-side}}$, the overall behaviour of $\frac{2}{\langle N_{\text{part}} \rangle} \langle dN_{\text{ch}}/d\eta \rangle$ as a function of $\langle N_{\text{part}} \rangle$ is flat, and agrees with the pp measurement at 8 TeV.

Acknowledgements

The ALICE Collaboration would like to thank J. Albacete, W.-T. Deng, A. Dumitru, T. Pierog and K. Werner for helpful discussions on their model predictions.

The ALICE Collaboration would like to thank all its engineers and technicians for their invaluable contributions to the construction of the experiment and the CERN accelerator teams for the outstanding performance of the LHC complex. The ALICE Collaboration gratefully acknowledges the resources and support provided by all Grid centres and the Worldwide LHC Computing Grid (WLCG) collaboration. The ALICE Collaboration acknowledges the following funding agencies for their support in building and running the ALICE detector: A. I. Alikhanyan National Science Laboratory (Yerevan Physics Institute) Foundation (ANSL), State Committee of Science and World Federation of Scientists (WFS), Armenia; Austrian Academy of Sciences and Nationalstiftung für Forschung, Technologie und Entwicklung, Austria; Ministry of Communications and High Technologies, National Nuclear Research Center, Azerbaijan; Conselho Nacional de Desenvolvimento Científico e Tecnológico (CNPq), Universidade Federal do Rio Grande do Sul (UFRGS), Financiadora de Estudos e Projetos (Finep) and Fundação de Amparo à Pesquisa do Estado de São Paulo (FAPESP), Brazil; Ministry of Science & Technology of China (MSTC), National Natural Science Foundation of China (NSFC) and Ministry of Education of China (MOEC), China; Ministry of Science and Education, Croatia; Centro de Aplicaciones Tecnológicas y Desarrollo Nuclear (CEADEN), Cubaenergía, Cuba; Ministry of Education, Youth and Sports of the Czech Republic, Czech Republic; The Danish Council for Independent Research — Natural Sciences, the Carlsberg Foundation and Danish National Research Foundation (DNRF), Denmark; Helsinki Institute of Physics (HIP), Finland; Commissariat à l’Energie Atomique (CEA) and Institut National de Physique Nucléaire et de Physique des Particules (IN2P3) and Centre National de la Recherche Scientifique (CNRS), France; Bundesministerium für Bildung, Wissenschaft, Forschung und Technologie (BMBF) and GSI Helmholtzzentrum für Schwerionenforschung GmbH, Germany; General Secretariat for Research and Technology, Ministry of Education, Research and Religions, Greece; National Research, Development and Innovation Office, Hungary; Department of Atomic Energy Government of India (DAE), Department of Science and Technology, Government of India (DST), University Grants Commission, Government of India (UGC) and Council of Scientific and Industrial Research (CSIR), India; Indonesian Institute of Science, Indonesia; Centro Fermi - Museo Storico della Fisica e Centro Studi e Ricerche Enrico Fermi and Istituto Nazionale di Fisica Nucleare (INFN), Italy; Institute for Innovative Science and Technology, Nagasaki Institute of Applied Science (IIST), Japan Society for the Promotion of Science (JSPS) KAKENHI and Japanese Ministry of Education, Culture, Sports, Science and Technology (MEXT), Japan; Consejo Nacional de Ciencia (CONACYT) y Tecnología, through Fondo de Cooperación Internacional en Ciencia y Tecnología (FONCICYT) and Dirección General de Asuntos del Personal Académico (DGAPA), Mexico; Nederlandse Organisatie voor Wetenschappelijk Onderzoek (NWO), Netherlands; The Research Council of Norway, Norway; Commission on Science and Technology for Sustainable Development in the South (COMSATS), Pakistan; Pontificia Universidad Católica del Perú, Peru; Ministry of Science and Higher Education and National Science Centre, Poland; Korea Institute of Science and Technology Information and National Research Foundation of Korea (NRF), Republic of Korea; Ministry of Education and Scientific Research, Institute of Atomic Physics and Romanian National Agency for Science, Technology and Innovation, Romania; Joint Institute for Nuclear Research (JINR), Ministry of Education and Science of the Russian Federation, National Research Cen-

the Kurchatov Institute, Russian Science Foundation and Russian Foundation for Basic Research, Russia; Ministry of Education, Science, Research and Sport of the Slovak Republic, Slovakia; National Research Foundation of South Africa, South Africa; Swedish Research Council (VR) and Knut & Alice Wallenberg Foundation (KAW), Sweden; European Organization for Nuclear Research, Switzerland; National Science and Technology Development Agency (NSDTA), Suranaree University of Technology (SUT) and Office of the Higher Education Commission under NRU project of Thailand, Thailand; Turkish Atomic Energy Agency (TAEK), Turkey; National Academy of Sciences of Ukraine, Ukraine; Science and Technology Facilities Council (STFC), United Kingdom; National Science Foundation of the United States of America (NSF) and United States Department of Energy, Office of Nuclear Physics (DOE NP), United States of America.

References

- [1] **ALICE** Collaboration, B. Abelev *et al.*, “Long-range angular correlations on the near and away side in p-Pb collisions at $\sqrt{s_{NN}} = 5.02$ TeV”, *Phys. Lett.* **B719** (2013), arXiv:1212.2001 [nucl-ex].
- [2] **ATLAS** Collaboration, G. Aad *et al.*, “Observation of Associated Near-Side and Away-Side Long-Range Correlations in $\sqrt{s_{NN}} = 5.02$ TeV Proton-Lead Collisions with the ATLAS Detector”, *Phys. Rev. Lett.* **110** no. 18, (2013), arXiv:1212.5198 [hep-ex].
- [3] **CMS** Collaboration, S. Chatrchyan *et al.*, “Observation of long-range near-side angular correlations in proton-lead collisions at the LHC”, *Phys. Lett.* **B718** (2013), arXiv:1210.5482 [nucl-ex].
- [4] **ALICE** Collaboration, B. Abelev *et al.*, “Multiplicity dependence of the average transverse momentum in pp, p-Pb, and Pb-Pb collisions at the LHC”, *Phys. Lett.* **B727** (2013), arXiv:1307.1094 [nucl-ex].
- [5] **ALICE** Collaboration, B. Abelev *et al.*, “Long-range angular correlations of π , K and p in p-Pb collisions at $\sqrt{s_{NN}} = 5.02$ TeV”, *Phys. Lett.* **B726** (2013), arXiv:1307.3237 [nucl-ex].
- [6] **ALICE** Collaboration, B. Abelev *et al.*, “Multiplicity Dependence of Pion, Kaon, Proton and Lambda Production in p-Pb Collisions at $\sqrt{s_{NN}} = 5.02$ TeV”, *Phys. Lett.* **B728** (2014), arXiv:1307.6796 [nucl-ex].
- [7] **ALICE** Collaboration, B. Abelev *et al.*, “Multiparticle azimuthal correlations in p-Pb and Pb-Pb collisions at the CERN Large Hadron Collider”, *Phys. Rev.* **C90** no. 5, (2014), arXiv:1406.2474 [nucl-ex].
- [8] **ALICE** Collaboration, J. Adam *et al.*, “Forward-central two-particle correlations in p-Pb collisions at $\sqrt{s_{NN}} = 5.02$ TeV”, *Phys. Lett.* **B753** (2016), arXiv:1506.08032 [nucl-ex].
- [9] **CMS** Collaboration, V. Khachatryan *et al.*, “Evidence for Collective Multiparticle Correlations in p-Pb Collisions”, *Phys. Rev. Lett.* **115** no. 1, (2015), arXiv:1502.05382 [nucl-ex].
- [10] J. L. Nagle and W. A. Zajc, “Small System Collectivity in Relativistic Hadronic and Nuclear Collisions”, *Ann. Rev. Nucl. Part. Sci.* **68** (2018), arXiv:1801.03477 [nucl-ex].
- [11] **ALICE** Collaboration, S. Acharya *et al.*, “The ALICE definition of primary particles”, June, 2017. <http://cds.cern.ch/record/2270008>.
- [12] W.-T. Deng, X.-N. Wang, and R. Xu, “Hadron production in p+p, p+Pb, and Pb+Pb collisions with the HIJING 2.0 model at energies available at the CERN Large Hadron Collider”, *Phys. Rev.* **C83** (2011), arXiv:1008.1841 [hep-ph].

- [13] R. Xu, W.-T. Deng, and X.-N. Wang, “Nuclear modification of high- p_T hadron spectra in p+A collisions at LHC”, *Phys. Rev.* **C86** (2012), arXiv:1204.1998 [nucl-th].
- [14] H. J. Drescher, M. Hladik, S. Ostapchenko, T. Pierog, and K. Werner, “Parton based Gribov-Regge theory”, *Phys. Rept.* **350** (2001), arXiv:hep-ph/0007198 [hep-ph].
- [15] K. Werner, I. Karpenko, T. Pierog, M. Bleicher, and K. Mikhailov, “Event-by-Event Simulation of the Three-Dimensional Hydrodynamic Evolution from Flux Tube Initial Conditions in Ultrarelativistic Heavy Ion Collisions”, *Phys. Rev.* **C82** (2010), arXiv:1004.0805 [nucl-th].
- [16] K. Werner, B. Guiot, I. Karpenko, and T. Pierog, “Analysing radial flow features in p-Pb and p-p collisions at several TeV by studying identified particle production in EPOS3”, *Phys. Rev.* **C89** no. 6, (2014), arXiv:1312.1233 [nucl-th].
- [17] T. Pierog, I. Karpenko, J. M. Katzy, E. Yatsenko, and K. Werner, “EPOS LHC: Test of collective hadronization with data measured at the CERN Large Hadron Collider”, *Phys. Rev.* **C92** no. 3, (2015), arXiv:1306.0121 [hep-ph].
- [18] J. L. Albacete and A. Dumitru, “A model for gluon production in heavy-ion collisions at the LHC with rcBK unintegrated gluon densities”, arXiv:1011.5161 [hep-ph].
- [19] J. L. Albacete, A. Dumitru, H. Fujii, and Y. Nara, “CGC predictions for p + Pb collisions at the LHC”, *Nucl. Phys.* **A897** (2013), arXiv:1209.2001 [hep-ph].
- [20] D. Kharzeev, E. Levin, and M. Nardi, “QCD saturation and deuteron nucleus collisions”, *Nucl. Phys.* **A730** (2004), arXiv:hep-ph/0212316 [hep-ph]. [Erratum: Nucl. Phys.A743,329(2004)].
- [21] A. Dumitru, D. E. Kharzeev, E. M. Levin, and Y. Nara, “Gluon Saturation in pA Collisions at the LHC: KLN Model Predictions For Hadron Multiplicities”, *Phys. Rev.* **C85** (2012), arXiv:1111.3031 [hep-ph].
- [22] ALICE Collaboration, K. Aamodt *et al.*, “The ALICE experiment at the CERN LHC”, *JINST* **3** (2008).
- [23] ALICE Collaboration, B. Abelev *et al.*, “Performance of the ALICE Experiment at the CERN LHC”, *Int. J. Mod. Phys.* **A29** (2014), arXiv:1402.4476 [nucl-ex].
- [24] ALICE Collaboration, E. Abbas *et al.*, “Performance of the ALICE VZERO system”, *JINST* **8** (2013), arXiv:1306.3130 [nucl-ex].
- [25] ALICE Collaboration, M. Gallio, W. Klempt, L. Leistam, J. De Groot, and J. Schkraft, *ALICE Zero-Degree Calorimeter (ZDC): Technical Design Report*. Technical Design Report ALICE. CERN, Geneva, 1999. <https://cds.cern.ch/record/381433>.
- [26] S. Roesler, R. Engel, and J. Ranft, “The Monte Carlo event generator DPMJET-III”, in *Advanced Monte Carlo for radiation physics, particle transport simulation and applications. Proceedings, Conference, MC2000, Lisbon, Portugal, October 23-26, 2000*, pp. 1033–1038. 2000. arXiv:hep-ph/0012252 [hep-ph]. <http://www-public.slac.stanford.edu/sciDoc/docMeta.aspx?slacPubNumber=SLAC-PUB-8740>.
- [27] X.-N. Wang and M. Gyulassy, “HIJING: A Monte Carlo model for multiple jet production in p p, p A and A A collisions”, *Phys. Rev.* **D44** (1991).
- [28] R. Brun, F. Bruyant, F. Carminati, S. Giani, M. Maire, A. McPherson, G. Patrick, and L. Urban, “GEANT Detector Description and Simulation Tool”.

- [29] M. L. Miller, K. Reygers, S. J. Sanders, and P. Steinberg, “Glauber modeling in high energy nuclear collisions”, *Ann. Rev. Nucl. Part. Sci.* **57** (2007), arXiv:nucl-ex/0701025 [nucl-ex].
- [30] C. Loizides, J. Kamin, and D. d’Enterria, “Improved Monte Carlo Glauber predictions at present and future nuclear colliders”, *Phys. Rev.* **C97** (2018), arXiv:1710.07098 [nucl-ex].
- [31] ALICE Collaboration, J. Adam *et al.*, “Centrality dependence of particle production in p-Pb collisions at $\sqrt{s_{NN}} = 5.02$ TeV”, *Phys. Rev.* **C91** no. 6, (2015), arXiv:1412.6828 [nucl-ex].
- [32] H. De Vries, C. W. De Jager, and C. De Vries, “Nuclear charge and magnetization density distribution parameters from elastic electron scattering”, *Atom. Data Nucl. Data Tabl.* **36** (1987).
- [33] A. Bialas and A. Bzdak, “Wounded quarks and diquarks in high energy collisions”, *Phys. Rev.* **C77** (2008), arXiv:0707.3720 [hep-ph].
- [34] ALICE Collaboration, B. Abelev *et al.*, “Pseudorapidity density of charged particles in p + Pb collisions at $\sqrt{s_{NN}} = 5.02$ TeV”, *Phys. Rev. Lett.* **110** no. 3, (2013), arXiv:1210.3615 [nucl-ex].
- [35] ALICE Collaboration, J. Adam *et al.*, “Enhanced production of multi-strange hadrons in high-multiplicity proton-proton collisions”, *Nature Phys.* **13** (2017), arXiv:1606.07424 [nucl-ex].
- [36] CMS Collaboration, A. M. Sirunyan *et al.*, “Pseudorapidity distributions of charged hadrons in proton-lead collisions at $\sqrt{s_{NN}} = 5.02$ and 8.16 TeV”, *JHEP* **01** (2018), arXiv:1710.09355 [hep-ex].
- [37] PHOBOS Collaboration, B. B. Back *et al.*, “Pseudorapidity distribution of charged particles in d + Au collisions at $s(NN)^{1/2} = 200$ -GeV”, *Phys. Rev. Lett.* **93** (2004), arXiv:nucl-ex/0311009 [nucl-ex].
- [38] ALICE Collaboration, J. Adam *et al.*, “Charged-particle multiplicities in proton-proton collisions at $\sqrt{s} = 0.9$ to 8 TeV”, *Eur. Phys. J.* **C77** no. 1, (2017), arXiv:1509.07541 [nucl-ex].
- [39] CMS Collaboration, V. Khachatryan *et al.*, “Pseudorapidity distribution of charged hadrons in proton-proton collisions at $\sqrt{s} = 13$ TeV”, *Phys. Lett.* **B751** (2015), arXiv:1507.05915 [hep-ex].
- [40] ALICE Collaboration, J. Adam *et al.*, “Pseudorapidity and transverse-momentum distributions of charged particles in proton-proton collisions at $\sqrt{s} = 13$ TeV”, *Phys. Lett.* **B753** (2016), arXiv:1509.08734 [nucl-ex].
- [41] ALICE Collaboration, S. Acharya *et al.*, “Centrality and pseudorapidity dependence of the charged-particle multiplicity density in Xe-Xe collisions at $\sqrt{s_{NN}} = 5.44$ TeV”, arXiv:1805.04432 [nucl-ex].
- [42] ALICE Collaboration, J. Adam *et al.*, “Centrality dependence of the charged-particle multiplicity density at midrapidity in Pb-Pb collisions at $\sqrt{s_{NN}} = 5.02$ TeV”, *Phys. Rev. Lett.* **116** no. 22, (2016), arXiv:1512.06104 [nucl-ex].
- [43] ALICE Collaboration, K. Aamodt *et al.*, “Centrality dependence of the charged-particle multiplicity density at mid-rapidity in Pb-Pb collisions at $\sqrt{s_{NN}} = 2.76$ TeV”, *Phys. Rev. Lett.* **106** (2011), arXiv:1012.1657 [nucl-ex].

- [44] **ATLAS** Collaboration, G. Aad *et al.*, “Measurement of the centrality dependence of the charged particle pseudorapidity distribution in lead-lead collisions at $\sqrt{s_{NN}} = 2.76$ TeV with the ATLAS detector”, *Phys. Lett.* **B710** (2012), arXiv:1108.6027 [hep-ex].
- [45] **CMS** Collaboration, S. Chatrchyan *et al.*, “Dependence on pseudorapidity and centrality of charged hadron production in PbPb collisions at a nucleon-nucleon centre-of-mass energy of 2.76 TeV”, *JHEP* **08** (2011), arXiv:1107.4800 [nucl-ex].
- [46] **NA50** Collaboration, M. C. Abreu *et al.*, “Scaling of charged particle multiplicity in Pb Pb collisions at SPS energies”, *Phys. Lett.* **B530** (2002) .
- [47] **BRAHMS** Collaboration, I. G. Bearden *et al.*, “Charged particle densities from Au+Au collisions at $s(NN)^{1/2} = 130$ -GeV”, *Phys. Lett.* **B523** (2001), arXiv:nucl-ex/0108016 [nucl-ex].
- [48] **BRAHMS** Collaboration, I. G. Bearden *et al.*, “Pseudorapidity distributions of charged particles from Au+Au collisions at the maximum RHIC energy”, *Phys. Rev. Lett.* **88** (2002), arXiv:nucl-ex/0112001 [nucl-ex].
- [49] **PHENIX** Collaboration, K. Adcox *et al.*, “Centrality dependence of charged particle multiplicity in Au - Au collisions at $S(NN)^{1/2} = 130$ -GeV”, *Phys. Rev. Lett.* **86** (2001), arXiv:nucl-ex/0012008 [nucl-ex].
- [50] **PHOBOS** Collaboration, B. Alver *et al.*, “Phobos results on charged particle multiplicity and pseudorapidity distributions in Au+Au, Cu+Cu, d+Au, and p+p collisions at ultra-relativistic energies”, *Phys. Rev.* **C83** (2011), arXiv:1011.1940 [nucl-ex].
- [51] **STAR** Collaboration, B. I. Abelev *et al.*, “Systematic Measurements of Identified Particle Spectra in pp, d^+ Au and Au+Au Collisions from STAR”, *Phys. Rev.* **C79** (2009), arXiv:0808.2041 [nucl-ex].
- [52] L. D. McLerran and R. Venugopalan, “Computing quark and gluon distribution functions for very large nuclei”, *Phys. Rev.* **D49** (1994), arXiv:hep-ph/9309289 [hep-ph].
- [53] J. L. Albacete *et al.*, “Predictions for p+Pb Collisions at $\sqrt{s_{NN}} = 5$ TeV”, *Int. J. Mod. Phys.* **E22** (2013), arXiv:1301.3395 [hep-ph].
- [54] S. Eremín and S. Voloshin, “Nucleon participants or quark participants?”, *Phys. Rev.* **C67** (2003), arXiv:nucl-th/0302071 [nucl-th].
- [55] C. Loizides, “Glauber modeling of high-energy nuclear collisions at the subnucleon level”, *Phys. Rev.* **C94** no. 2, (2016), arXiv:1603.07375 [nucl-ex].
- [56] **PHENIX** Collaboration, A. Adare *et al.*, “Transverse energy production and charged-particle multiplicity at midrapidity in various systems from $\sqrt{s_{NN}} = 7.7$ to 200 GeV”, *Phys. Rev.* **C93** no. 2, (2016), arXiv:1509.06727 [nucl-ex].

A The ALICE Collaboration

S. Acharya¹⁴⁰, F.T.-. Acosta²⁰, D. Adamová⁹³, S.P. Adhya¹⁴⁰, A. Adler⁷⁴, J. Adolfsson⁸⁰, M.M. Aggarwal⁹⁸, G. Aglieri Rinella³⁴, M. Agnello³¹, Z. Ahammed¹⁴⁰, S. Ahmad¹⁷, S.U. Ahn⁷⁶, S. Aiola¹⁴⁵, A. Akindinov⁶⁴, M. Al-Turany¹⁰⁴, S.N. Alam¹⁴⁰, D.S.D. Albuquerque¹²¹, D. Aleksandrov⁸⁷, B. Alessandro⁵⁸, H.M. Alfanda⁶, R. Alfaro Molina⁷², Y. Ali¹⁵, A. Alici^{10,53,27}, A. Alkin², J. Alme²², T. Alt⁶⁹, L. Altenkamper²², I. Altsybeev¹¹¹, M.N. Anaam⁶, C. Andrei⁴⁷, D. Andreou³⁴, H.A. Andrews¹⁰⁸, A. Andronic^{143,104}, M. Angeletti³⁴, V. Anguelov¹⁰², C. Anson¹⁶, T. Antičić¹⁰⁵, F. Antinori⁵⁶, P. Antonioli⁵³, R. Anwar¹²⁵, N. Apadula⁷⁹, L. Aphecetche¹¹³, H. Appelshäuser⁶⁹, S. Arcelli²⁷, R. Arnaldi⁵⁸, M. Arratia⁷⁹, I.C. Arsene²¹, M. Arslanok¹⁰², A. Augustinus³⁴, R. Averbeck¹⁰⁴, M.D. Azmi¹⁷, A. Badalá⁵⁵, Y.W. Baek^{40,60}, S. Bagnasco⁵⁸, R. Bailhache⁶⁹, R. Bala⁹⁹, A. Baldisseri¹³⁶, M. Ball⁴², R.C. Baral⁸⁵, R. Barbera²⁸, L. Barioglio²⁶, G.G. Barnaföldi¹⁴⁴, L.S. Barnby⁹², V. Barret¹³³, P. Bartalini⁶, K. Barth³⁴, E. Bartsch⁶⁹, N. Bastid¹³³, S. Basu¹⁴², G. Batigne¹¹³, B. Batyunya⁷⁵, P.C. Batzing²¹, D. Bauri⁴⁸, J.L. Bazo Alba¹⁰⁹, I.G. Bearden⁸⁸, H. Beck¹⁰², C. Bedda⁶³, N.K. Behera⁶⁰, I. Belikov¹³⁵, F. Bellini³⁴, H. Bello Martinez⁴⁴, R. Bellwied¹²⁵, L.G.E. Beltran¹¹⁹, V. Belyaev⁹¹, G. Bencedi¹⁴⁴, S. Beole²⁶, A. Bercuci⁴⁷, Y. Berdnikov⁹⁶, D. Berenyi¹⁴⁴, R.A. Bertens¹²⁹, D. Berzano⁵⁸, L. Betev³⁴, A. Bhasin⁹⁹, I.R. Bhat⁹⁹, H. Bhatt⁴⁸, B. Bhattacharjee⁴¹, A. Bianchi²⁶, L. Bianchi^{125,26}, N. Bianchi⁵¹, J. Bielčák³⁷, J. Bielčíková⁹³, A. Bilandzic^{116,103}, G. Biro¹⁴⁴, R. Biswas³, S. Biswas³, J.T. Blair¹¹⁸, D. Blau⁸⁷, C. Blume⁶⁹, G. Boca¹³⁸, F. Bock³⁴, A. Bogdanov⁹¹, L. Boldizsár¹⁴⁴, A. Bolozdynya⁹¹, M. Bombara³⁸, G. Bonomi¹³⁹, M. Bonora³⁴, H. Borel¹³⁶, A. Borissov^{143,102}, M. Borri¹²⁷, E. Botta²⁶, C. Bourjau⁸⁸, L. Bratrud⁶⁹, P. Braun-Munzinger¹⁰⁴, M. Bregant¹²⁰, T.A. Broker⁶⁹, M. Broz³⁷, E.J. Brucken⁴³, E. Bruna⁵⁸, G.E. Bruno³³, D. Budnikov¹⁰⁶, H. Buesching⁶⁹, S. Bufalino³¹, P. Buhler¹¹², P. Buncic³⁴, O. Busch^{132,i}, Z. Buthelezi⁷³, J.B. Butt¹⁵, J.T. Buxton⁹⁵, J. Cabala¹¹⁵, D. Caffarri⁸⁹, H. Caines¹⁴⁵, A. Caliva¹⁰⁴, E. Calvo Villar¹⁰⁹, R.S. Camacho⁴⁴, P. Camerini²⁵, A.A. Capon¹¹², F. Carnesecchi^{27,10}, J. Castillo Castellanos¹³⁶, A.J. Castro¹²⁹, E.A.R. Casula⁵⁴, C. Ceballos Sanchez^{8,52}, P. Chakraborty⁴⁸, S. Chandra¹⁴⁰, B. Chang¹²⁶, W. Chang⁶, S. Chapeland³⁴, M. Chartier¹²⁷, S. Chattopadhyay¹⁴⁰, S. Chattopadhyay¹⁰⁷, A. Chauvin²⁴, C. Cheshkov¹³⁴, B. Cheynis¹³⁴, V. Chibante Barroso³⁴, D.D. Chinellato¹²¹, S. Cho⁶⁰, P. Chochula³⁴, T. Chowdhury¹³³, P. Christakoglou⁸⁹, C.H. Christensen⁸⁸, P. Christiansen⁸⁰, T. Chujo¹³², C. Cicalo⁵⁴, L. Cifarelli^{10,27}, F. Cindolo⁵³, J. Cleymans¹²⁴, F. Colamaria⁵², D. Colella⁵², A. Collu⁷⁹, M. Colocci²⁷, M. Concas^{58,ii}, G. Conesa Balbastre⁷⁸, Z. Conesa del Valle⁶¹, J.G. Contreras³⁷, T.M. Cormier⁹⁴, Y. Corrales Morales⁵⁸, P. Cortese³², M.R. Cosentino¹²², F. Costa³⁴, S. Costanza¹³⁸, J. Crkovská⁶¹, P. Crochet¹³³, E. Cuautle⁷⁰, L. Cunqueiro⁹⁴, D. Dabrowski¹⁴¹, T. Dahms^{103,116}, A. Dainese⁵⁶, F.P.A. Damas^{136,113}, S. Dani⁶⁶, M.C. Danisch¹⁰², A. Danu⁶⁸, D. Das¹⁰⁷, I. Das¹⁰⁷, S. Das³, A. Dash⁸⁵, S. Dash⁴⁸, S. De⁴⁹, A. De Caro³⁰, G. de Cataldo⁵², C. de Conti¹²⁰, J. de Cuveland³⁹, A. De Falco²⁴, D. De Gruttola^{10,30}, N. De Marco⁵⁸, S. De Pasquale³⁰, R.D. De Souza¹²¹, H.F. Degenhardt¹²⁰, A. Deisting^{102,104}, A. Deloff⁸⁴, S. Delsanto²⁶, P. Dhankher⁴⁸, D. Di Bari³³, A. Di Mauro³⁴, R.A. Diaz⁸, T. Dietel¹²⁴, P. Dillenseger⁶⁹, Y. Ding⁶, R. Divià³⁴, Ø. Djuvland²², A. Dobrin³⁴, D. Domenicis Gimenez¹²⁰, B. Dönigus⁶⁹, O. Dordic²¹, A.K. Dubey¹⁴⁰, A. Dubla¹⁰⁴, S. Dudi⁹⁸, A.K. Duggal⁹⁸, M. Dukhishyam⁸⁵, P. Dupieux¹³³, R.J. Ehlers¹⁴⁵, D. Elia⁵², H. Engel⁷⁴, E. Epple¹⁴⁵, B. Erazmus¹¹³, F. Erhardt⁹⁷, A. Erokhin¹¹¹, M.R. Ersdal²², B. Espagnon⁶¹, G. Eulisse³⁴, J. Eum¹⁸, D. Evans¹⁰⁸, S. Evdokimov⁹⁰, L. Fabbietti^{103,116}, M. Faggin²⁹, J. Faivre⁷⁸, A. Fantoni⁵¹, M. Fasel⁹⁴, L. Feldkamp¹⁴³, A. Feliciello⁵⁸, G. Feofilov¹¹¹, A. Fernández Téllez⁴⁴, A. Ferrero¹³⁶, A. Ferretti²⁶, A. Festanti³⁴, V.J.G. Feuillard¹⁰², J. Figiel¹¹⁷, S. Filchagin¹⁰⁶, D. Finogeev⁶², F.M. Fionda²², G. Fiorenza⁵², F. Flor¹²⁵, M. Floris³⁴, S. Foertsch⁷³, P. Foka¹⁰⁴, S. Fokin⁸⁷, E. Fragiaco⁵⁹, A. Francisco¹¹³, U. Frankenfeld¹⁰⁴, G.G. Fronze²⁶, U. Fuchs³⁴, C. Furget⁷⁸, A. Furs⁶², M. Fusco Girard³⁰, J.J. Gaardhøje⁸⁸, M. Gagliardi²⁶, A.M. Gago¹⁰⁹, K. Gajdosova^{37,88}, C.D. Galvan¹¹⁹, P. Ganoti⁸³, C. Garabatos¹⁰⁴, E. Garcia-Solis¹¹, K. Garg²⁸, C. Gargiulo³⁴, K. Garner¹⁴³, P. Gasik^{103,116}, E.F. Gauger¹¹⁸, M.B. Gay Ducati⁷¹, M. Germain¹¹³, J. Ghosh¹⁰⁷, P. Ghosh¹⁴⁰, S.K. Ghosh³, P. Gianotti⁵¹, P. Giubellino^{104,58}, P. Giubileo²⁹, P. Glässel¹⁰², D.M. Gómez Coral⁷², A. Gomez Ramirez⁷⁴, V. Gonzalez¹⁰⁴, P. González-Zamora⁴⁴, S. Gorbunov³⁹, L. Görlich¹¹⁷, S. Gotovac³⁵, V. Grabski⁷², L.K. Graczykowski¹⁴¹, K.L. Graham¹⁰⁸, L. Greiner⁷⁹, A. Grelli⁶³, C. Grigoras³⁴, V. Grigoriev⁹¹, A. Grigoryan¹, S. Grigoryan⁷⁵, J.M. Gronefeld¹⁰⁴, F. Grosa³¹, J.F. Grosse-Oetringhaus³⁴, R. Grosso¹⁰⁴, R. Guernane⁷⁸, B. Guerzoni²⁷, M. Guittiere¹¹³, K. Gulbrandsen⁸⁸, T. Gunji¹³¹, A. Gupta⁹⁹, R. Gupta⁹⁹, I.B. Guzman⁴⁴, R. Haake^{145,34}, M.K. Habib¹⁰⁴, C. Hadjidakis⁶¹, H. Hamagaki⁸¹, G. Hamar¹⁴⁴, M. Hamid⁶, J.C. Hamon¹³⁵, R. Hannigan¹¹⁸, M.R. Haque⁶³, A. Harlanderova¹⁰⁴, J.W. Harris¹⁴⁵, A. Harton¹¹, H. Hassan⁷⁸, D. Hatzifotiadiou^{53,10}, P. Hauer⁴², S. Hayashi¹³¹, S.T. Heckel⁶⁹, E. Hellbär⁶⁹, H. Helstrup³⁶, A. Hergelegiu⁴⁷, E.G. Hernandez⁴⁴, G. Herrera Corral⁹, F. Herrmann¹⁴³, K.F. Hetland³⁶, T.E. Hilden⁴³, H. Hillemanns³⁴, C. Hills¹²⁷, B. Hippolyte¹³⁵, B. Hohlweger¹⁰³, D. Horak³⁷, S. Hornung¹⁰⁴, R. Hosokawa¹³², J. Hota⁶⁶, P. Hristov³⁴, C. Huang⁶¹, C. Hughes¹²⁹, P. Huhn⁶⁹, T.J. Humanic⁹⁵, H. Hushnud¹⁰⁷,

L.A. Husova¹⁴³, N. Hussain⁴¹, T. Hussain¹⁷, D. Hutter³⁹, D.S. Hwang¹⁹, J.P. Iddon¹²⁷, R. Ilkaev¹⁰⁶, M. Inaba¹³², M. Ippolitov⁸⁷, M.S. Islam¹⁰⁷, M. Ivanov¹⁰⁴, V. Ivanov⁹⁶, V. Izucheev⁹⁰, B. Jacak⁷⁹, N. Jacazio²⁷, P.M. Jacobs⁷⁹, M.B. Jadhav⁴⁸, S. Jadlovská¹¹⁵, J. Jadlovsky¹¹⁵, S. Jaelani⁶³, C. Jahnke^{120,116}, M.J. Jakubowska¹⁴¹, M.A. Janik¹⁴¹, M. Jercic⁹⁷, O. Jevons¹⁰⁸, R.T. Jimenez Bustamante¹⁰⁴, M. Jin¹²⁵, P.G. Jones¹⁰⁸, A. Jusko¹⁰⁸, P. Kalinák⁶⁵, A. Kalweit³⁴, J.H. Kang¹⁴⁶, V. Kaplin⁹¹, S. Kar⁶, A. Karasu Uysal⁷⁷, O. Karavichev⁶², T. Karavicheva⁶², P. Karczmarczyk³⁴, E. Karpechev⁶², U. Keschull⁷⁴, R. Keidel⁴⁶, M. Keil³⁴, B. Ketzer⁴², Z. Khabanova⁸⁹, A.M. Khan⁶, S. Khan¹⁷, S.A. Khan¹⁴⁰, A. Khanzadeev⁹⁶, Y. Kharlov⁹⁰, A. Khatun¹⁷, A. Khuntia⁴⁹, M.M. Kielbowicz¹¹⁷, B. Kileng³⁶, B. Kim⁶⁰, B. Kim¹³², D. Kim¹⁴⁶, D.J. Kim¹²⁶, E.J. Kim¹³, H. Kim¹⁴⁶, J.S. Kim⁴⁰, J. Kim¹⁰², J. Kim¹³, M. Kim^{60,102}, S. Kim¹⁹, T. Kim¹⁴⁶, T. Kim¹⁴⁶, K. Kindra⁹⁸, S. Kirsch³⁹, I. Kisel³⁹, S. Kiselev⁶⁴, A. Kisiel¹⁴¹, J.L. Klay⁵, C. Klein⁶⁹, J. Klein⁵⁸, S. Klein⁷⁹, C. Klein-Bösing¹⁴³, S. Klewin¹⁰², A. Kluge³⁴, M.L. Knichel³⁴, A.G. Knospe¹²⁵, C. Kobdaj¹¹⁴, M. Kofarago¹⁴⁴, M.K. Köhler¹⁰², T. Kollegger¹⁰⁴, N. Kondratyeva⁹¹, E. Kondratyuk⁹⁰, P.J. Konopka³⁴, M. Konyushikhin¹⁴², L. Koska¹¹⁵, O. Kovalenko⁸⁴, V. Kovalenko¹¹¹, M. Kowalski¹¹⁷, I. Králik⁶⁵, A. Kravčáková³⁸, L. Kreis¹⁰⁴, M. Krivda^{108,65}, F. Krizek⁹³, M. Krüger⁶⁹, E. Kryshen⁹⁶, M. Krzewicki³⁹, A.M. Kubera⁹⁵, V. Kučera^{93,60}, C. Kuhn¹³⁵, P.G. Kuijter⁸⁹, J. Kumar⁴⁸, L. Kumar⁹⁸, S. Kumar⁴⁸, S. Kundu⁸⁵, P. Kurashvili⁸⁴, A. Kurepin⁶², A.B. Kurepin⁶², S. Kushpil⁹³, J. Kvapil¹⁰⁸, M.J. Kweon⁶⁰, Y. Kwon¹⁴⁶, S.L. La Pointe³⁹, P. La Rocca²⁸, Y.S. Lai⁷⁹, R. Langoy¹²³, K. Lapidus^{34,145}, A. Lardeux²¹, P. Larionov⁵¹, E. Laudi³⁴, R. Lavicka³⁷, T. Lazareva¹¹¹, R. Lea²⁵, L. Leardini¹⁰², S. Lee¹⁴⁶, F. Lehas⁸⁹, S. Lehner¹¹², J. Lehrbach³⁹, R.C. Lemmon⁹², I. León Monzón¹¹⁹, P. Lévai¹⁴⁴, X. Li¹², X.L. Li⁶, J. Lien¹²³, R. Lietava¹⁰⁸, B. Lim¹⁸, S. Lindal²¹, V. Lindenstruth³⁹, S.W. Lindsay¹²⁷, C. Lippmann¹⁰⁴, M.A. Lisa⁹⁵, V. Litichevskyi⁴³, A. Liu⁷⁹, H.M. Ljunggren⁸⁰, W.J. Llope¹⁴², D.F. Lodato⁶³, V. Loginov⁹¹, C. Loizides⁹⁴, P. Loncar³⁵, X. Lopez¹³³, E. López Torres⁸, P. Luettig⁶⁹, J.R. Luhder¹⁴³, M. Lunardon²⁹, G. Luparello⁵⁹, M. Lupi³⁴, A. Maevskaya⁶², M. Mager³⁴, S.M. Mahmood²¹, A. Maire¹³⁵, R.D. Majka¹⁴⁵, M. Malaev⁹⁶, Q.W. Malik²¹, L. Malinina^{75,iii}, D. Mal'Kevich⁶⁴, P. Malzacher¹⁰⁴, A. Mamonov¹⁰⁶, V. Manko⁸⁷, F. Manso¹³³, V. Manzari⁵², Y. Mao⁶, M. Marchisone¹³⁴, J. Mareš⁶⁷, G.V. Margagliotti²⁵, A. Margotti⁵³, J. Margutti⁶³, A. Marín¹⁰⁴, C. Markert¹¹⁸, M. Marquard⁶⁹, N.A. Martin^{102,104}, P. Martinengo³⁴, J.L. Martinez¹²⁵, M.I. Martínez⁴⁴, G. Martínez García¹¹³, M. Martinez Pedreira³⁴, S. Masciocchi¹⁰⁴, M. Maserà²⁶, A. Masoni⁵⁴, L. Massacrier⁶¹, E. Masson¹¹³, A. Mastroserio^{52,137}, A.M. Mathis^{116,103}, P.F.T. Matuoka¹²⁰, A. Matyja^{117,129}, C. Mayer¹¹⁷, M. Mazzilli³³, M.A. Mazzoni⁵⁷, F. Meddi²³, Y. Melikyan⁹¹, A. Menchaca-Rocha⁷², E. Meninno³⁰, M. Meres¹⁴, S. Mhlanga¹²⁴, Y. Miake¹³², L. Micheletti²⁶, M.M. Mieskolainen⁴³, D.L. Mihaylov¹⁰³, K. Mikhaylov^{75,64}, A. Mischke⁶³, A.N. Mishra⁷⁰, D. Miśkowiec¹⁰⁴, J. Mitra¹⁴⁰, C.M. Mitu⁶⁸, N. Mohammadi³⁴, A.P. Mohanty⁶³, B. Mohanty⁸⁵, M. Mohisin Khan^{17,iv}, M.M. Mondal⁶⁶, C. Mordasini¹⁰³, D.A. Moreira De Godoy¹⁴³, L.A.P. Moreno⁴⁴, S. Moretto²⁹, A. Morreale¹¹³, A. Morsch³⁴, T. Mrnjavac³⁴, V. Muccifora⁵¹, E. Mudnic³⁵, D. Mühlheim¹⁴³, S. Muhuri¹⁴⁰, J.D. Mulligan¹⁴⁵, M.G. Munhoz¹²⁰, K. Mürning⁴², R.H. Munzer⁶⁹, H. Murakami¹³¹, S. Murray⁷³, L. Musa³⁴, J. Musinsky⁶⁵, C.J. Myers¹²⁵, J.W. Myrcha¹⁴¹, B. Naik⁴⁸, R. Nair⁸⁴, B.K. Nandi⁴⁸, R. Nania^{53,10}, E. Nappi⁵², M.U. Naru¹⁵, A.F. Nassirpour⁸⁰, H. Natal da Luz¹²⁰, C. Nattrass¹²⁹, S.R. Navarro⁴⁴, K. Nayak⁸⁵, R. Nayak⁴⁸, T.K. Nayak^{140,85}, S. Nazarenko¹⁰⁶, R.A. Negrao De Oliveira⁶⁹, L. Nellen⁷⁰, S.V. Nesbo³⁶, G. Neskovic³⁹, F. Ng¹²⁵, B.S. Nielsen⁸⁸, S. Nikolaev⁸⁷, S. Nikulin⁸⁷, V. Nikulin⁹⁶, F. Noferini^{10,53}, P. Nomokonov⁷⁵, G. Nooren⁶³, J.C.C. Noris⁴⁴, J. Norman⁷⁸, A. Nyanin⁸⁷, J. Nystrand²², M. Ogino⁸¹, A. Ohlson¹⁰², J. Olińczak¹⁴¹, A.C. Oliveira Da Silva¹²⁰, M.H. Oliver¹⁴⁵, J. Onderwaater¹⁰⁴, C. Oppedisano⁵⁸, R. Orava⁴³, M. Oravec¹¹⁵, A. Ortiz Velasquez⁷⁰, A. Oskarsson⁸⁰, J. Otwinowski¹¹⁷, K. Oyama⁸¹, Y. Pachmayer¹⁰², V. Pacik⁸⁸, D. Pagano¹³⁹, G. Paic⁷⁰, P. Palni⁶, J. Pan¹⁴², A.K. Pandey⁴⁸, S. Panebianco¹³⁶, V. Papikyan¹, P. Pareek⁴⁹, J. Park⁶⁰, J.E. Parkkila¹²⁶, S. Parmar⁹⁸, A. Passfeld¹⁴³, S.P. Pathak¹²⁵, R.N. Patra¹⁴⁰, B. Paul⁵⁸, H. Pei⁶, T. Peitzmann⁶³, X. Peng⁶, L.G. Pereira⁷¹, H. Pereira Da Costa¹³⁶, D. Peresunko⁸⁷, G.M. Perez⁸, E. Perez Lezama⁶⁹, V. Peskov⁶⁹, Y. Pestov⁴, V. Petráček³⁷, M. Petrovici⁴⁷, R.P. Pezzi⁷¹, S. Piano⁵⁹, M. Pikna¹⁴, P. Pillot¹¹³, L.O.D.L. Pimentel⁸⁸, O. Pinazza^{53,34}, L. Pinsky¹²⁵, S. Pisano⁵¹, D.B. Piyarathna¹²⁵, M. Płoskoń⁷⁹, M. Planinic⁹⁷, F. Pliquett⁶⁹, J. Pluta¹⁴¹, S. Pochybova¹⁴⁴, P.L.M. Podesta-Lerma¹¹⁹, M.G. Poghosyan⁹⁴, B. Polichtchouk⁹⁰, N. Poljak⁹⁷, W. Poonasawat¹¹⁴, A. Pop⁴⁷, H. Poppenborg¹⁴³, S. Porteboeuf-Houssais¹³³, V. Pozdniakov⁷⁵, S.K. Prasad³, R. Preghenella⁵³, F. Prino⁵⁸, C.A. Pruneau¹⁴², I. Pshenichnov⁶², M. Puccio²⁶, V. Punin¹⁰⁶, K. Puranapanda¹⁴⁰, J. Putschke¹⁴², R.E. Quishpe¹²⁵, S. Raha³, S. Rajput⁹⁹, J. Rak¹²⁶, A. Rakotozafindrabe¹³⁶, L. Ramello³², F. Rami¹³⁵, R. Raniwala¹⁰⁰, S. Raniwala¹⁰⁰, S.S. Räsänen⁴³, B.T. Rascanu⁶⁹, R. Rath⁴⁹, V. Ratza⁴², I. Ravasenga³¹, K.F. Read^{129,94}, K. Redlich^{84,v}, A. Rehman²², P. Reichelt⁶⁹, F. Reidt³⁴, X. Ren⁶, R. Renfordt⁶⁹, A. Reshetin⁶², J.-P. Revol¹⁰, K. Reygers¹⁰², V. Riabov⁹⁶, T. Richert^{88,80}, M. Richter²¹, P. Riedler³⁴, W. Riegler³⁴, F. Riggi²⁸, C. Ristea⁶⁸, S.P. Rode⁴⁹, M. Rodríguez Cahuantzi⁴⁴, K. Røed²¹, R. Rogalev⁹⁰, E. Rogochaya⁷⁵, D. Rohr³⁴, D. Röhrich²²,

P.S. Rokita¹⁴¹, F. Ronchetti⁵¹, E.D. Rosas⁷⁰, K. Roslon¹⁴¹, P. Rosnet¹³³, A. Rossi^{56,29}, A. Rotondi¹³⁸, F. Roukoutakis⁸³, A. Roy⁴⁹, P. Roy¹⁰⁷, O.V. Rueda⁷⁰, R. Rui²⁵, B. Rumyantsev⁷⁵, A. Rustamov⁸⁶, E. Ryabinkin⁸⁷, Y. Ryabov⁹⁶, A. Rybicki¹¹⁷, S. Saarinen⁴³, S. Sadhu¹⁴⁰, S. Sadovsky⁹⁰, K. Šafařík^{34,37}, S.K. Saha¹⁴⁰, B. Sahoo⁴⁸, P. Sahoo⁴⁹, R. Sahoo⁴⁹, S. Sahoo⁶⁶, P.K. Sahu⁶⁶, J. Saini¹⁴⁰, S. Sakai¹³², M.A. Saleh¹⁴², S. Sambyal⁹⁹, V. Samsonov^{91,96}, A. Sandoval⁷², A. Sarkar⁷³, D. Sarkar¹⁴⁰, N. Sarkar¹⁴⁰, P. Sarma⁴¹, V.M. Sarti¹⁰³, M.H.P. Sas⁶³, E. Scapparone⁵³, B. Schaefer⁹⁴, J. Schambach¹¹⁸, H.S. Scheid⁶⁹, C. Schiaua⁴⁷, R. Schicker¹⁰², C. Schmidt¹⁰⁴, H.R. Schmidt¹⁰¹, M.O. Schmidt¹⁰², M. Schmidt¹⁰¹, N.V. Schmidt^{69,94}, J. Schukraft^{88,34}, Y. Schutz^{135,34}, K. Schwarz¹⁰⁴, K. Schweda¹⁰⁴, G. Scioli²⁷, E. Scomparin⁵⁸, M. Šefčík³⁸, J.E. Seger¹⁶, Y. Sekiguchi¹³¹, D. Sekihata⁴⁵, I. Selyuzhenkov^{104,91}, S. Senyukov¹³⁵, E. Serradilla⁷², P. Sett⁴⁸, A. Sevcenco⁶⁸, A. Shabanov⁶², A. Shabetai¹¹³, R. Shahoyan³⁴, W. Shaikh¹⁰⁷, A. Shangaraev⁹⁰, A. Sharma⁹⁸, A. Sharma⁹⁹, M. Sharma⁹⁹, N. Sharma⁹⁸, A.I. Sheikh¹⁴⁰, K. Shigaki⁴⁵, M. Shimomura⁸², S. Shirinkin⁶⁴, Q. Shou^{6,110}, Y. Sibiriak⁸⁷, S. Siddhanta⁵⁴, T. Siemiarczuk⁸⁴, D. Silvermyr⁸⁰, G. Simatovic⁸⁹, G. Simonetti^{103,34}, R. Singh⁸⁵, R. Singh⁹⁹, V. Singhal¹⁴⁰, T. Sinha¹⁰⁷, B. Sitar¹⁴, M. Sitta³², T.B. Skaali²¹, M. Slupecki¹²⁶, N. Smirnov¹⁴⁵, R.J.M. Snellings⁶³, T.W. Snellman¹²⁶, J. Sochan¹¹⁵, C. Soncco¹⁰⁹, J. Song⁶⁰, A. Songmoolnak¹¹⁴, F. Soramel²⁹, S. Sorensen¹²⁹, F. Sozzi¹⁰⁴, I. Sputowska¹¹⁷, J. Stachel¹⁰², I. Stan⁶⁸, P. Stankus⁹⁴, E. Stenlund⁸⁰, D. Stocco¹¹³, M.M. Storetvedt³⁶, P. Strmen¹⁴, A.A.P. Suaide¹²⁰, T. Sugitate⁴⁵, C. Suire⁶¹, M. Suleymanov¹⁵, M. Suljic³⁴, R. Sultanov⁶⁴, M. Šumbera⁹³, S. Sumowidagdo⁵⁰, K. Suzuki¹¹², S. Swain⁶⁶, A. Szabo¹⁴, I. Szarka¹⁴, U. Tabassam¹⁵, J. Takahashi¹²¹, G.J. Tambave²², N. Tanaka¹³², M. Tarhini¹¹³, M.G. Tarzila⁴⁷, A. Tauro³⁴, G. Tejada Muñoz⁴⁴, A. Telesca³⁴, C. Terrevoli^{29,125}, D. Thakur⁴⁹, S. Thakur¹⁴⁰, D. Thomas¹¹⁸, F. Thoresen⁸⁸, R. Tieulent¹³⁴, A. Tikhonov⁶², A.R. Timmins¹²⁵, A. Toia⁶⁹, N. Topilskaya⁶², M. Toppi⁵¹, S.R. Torres¹¹⁹, S. Tripathy⁴⁹, T. Tripathy⁴⁸, S. Trogolo²⁶, G. Trombetta³³, L. Tropp³⁸, V. Trubnikov², W.H. Trzaska¹²⁶, T.P. Trzcinski¹⁴¹, B.A. Trzeciak⁶³, T. Tsuji¹³¹, A. Tumkin¹⁰⁶, R. Turrisi⁵⁶, T.S. Tveter²¹, K. Ullaland²², E.N. Umaka¹²⁵, A. Uras¹³⁴, G.L. Usai²⁴, A. Utrobicic⁹⁷, M. Vala^{38,115}, L. Valencia Palomo⁴⁴, N. Valle¹³⁸, N. van der Kolk⁶³, L.V.R. van Doremalen⁶³, J.W. Van Hoorne³⁴, M. van Leeuwen⁶³, P. Vande Vyvre³⁴, D. Varga¹⁴⁴, A. Vargas⁴⁴, M. Vargyas¹²⁶, R. Varma⁴⁸, M. Vasileiou⁸³, A. Vasiliev⁸⁷, O. Vázquez Doce^{103,116}, V. Vechernin¹¹¹, A.M. Veen⁶³, E. Vercellin²⁶, S. Vergara Limón⁴⁴, L. Vermunt⁶³, R. Vernet⁷, R. Vértesi¹⁴⁴, L. Vickovic³⁵, J. Viinikainen¹²⁶, Z. Vilakazi¹³⁰, O. Villalobos Baillie¹⁰⁸, A. Villatoro Tello⁴⁴, G. Vio⁵², A. Vinogradov⁸⁷, T. Virgili³⁰, V. Vislavicius⁸⁸, A. Vodopyanov⁷⁵, B. Volkel³⁴, M.A. Völkl¹⁰¹, K. Voloshin⁶⁴, S.A. Voloshin¹⁴², G. Volpe³³, B. von Haller³⁴, I. Vorobyev^{116,103}, D. Voscek¹¹⁵, J. Vrláková³⁸, B. Wagner²², M. Wang⁶, Y. Watanabe¹³², M. Weber¹¹², S.G. Weber¹⁰⁴, A. Wegrzynek³⁴, D.F. Weiser¹⁰², S.C. Wenzel³⁴, J.P. Wessels¹⁴³, U. Westerhoff¹⁴³, A.M. Whitehead¹²⁴, E. Widmann¹¹², J. Wiechula⁶⁹, J. Wikne²¹, G. Wilk⁸⁴, J. Wilkinson⁵³, G.A. Willems^{34,143}, E. Willsher¹⁰⁸, B. Windelband¹⁰², W.E. Witt¹²⁹, Y. Wu¹²⁸, R. Xu⁶, S. Yalcin⁷⁷, K. Yamakawa⁴⁵, S. Yano¹³⁶, Z. Yin⁶, H. Yokoyama^{63,132}, I.-K. Yoo¹⁸, J.H. Yoon⁶⁰, S. Yuan²², V. Yurchenko², V. Zaccolo^{25,58}, A. Zaman¹⁵, C. Zampolli³⁴, H.J.C. Zanolli¹²⁰, N. Zardoshti^{108,34}, A. Zarochentsev¹¹¹, P. Závada⁶⁷, N. Zaviyalov¹⁰⁶, H. Zbroszczyk¹⁴¹, M. Zhalov⁹⁶, X. Zhang⁶, Y. Zhang⁶, Z. Zhang^{6,133}, C. Zhao²¹, V. Zherebchevskii¹¹¹, N. Zhigareva⁶⁴, D. Zhou⁶, Y. Zhou⁸⁸, Z. Zhou²², H. Zhu⁶, J. Zhu⁶, Y. Zhu⁶, A. Zichichi^{27,10}, M.B. Zimmermann³⁴, G. Zinovjev², N. Zurlo¹³⁹,

Affiliation notes

ⁱ Deceased

ⁱⁱ Dipartimento DET del Politecnico di Torino, Turin, Italy

ⁱⁱⁱ M.V. Lomonosov Moscow State University, D.V. Skobeltsyn Institute of Nuclear Physics, Moscow, Russia

^{iv} Department of Applied Physics, Aligarh Muslim University, Aligarh, India

^v Institute of Theoretical Physics, University of Wrocław, Poland

Collaboration Institutes

¹ A.I. Alikhanyan National Science Laboratory (Yerevan Physics Institute) Foundation, Yerevan, Armenia

² Bogolyubov Institute for Theoretical Physics, National Academy of Sciences of Ukraine, Kiev, Ukraine

³ Bose Institute, Department of Physics and Centre for Astroparticle Physics and Space Science (CAPSS), Kolkata, India

⁴ Budker Institute for Nuclear Physics, Novosibirsk, Russia

⁵ California Polytechnic State University, San Luis Obispo, California, United States

⁶ Central China Normal University, Wuhan, China

⁷ Centre de Calcul de l'IN2P3, Villeurbanne, Lyon, France

- ⁸ Centro de Aplicaciones Tecnológicas y Desarrollo Nuclear (CEADEN), Havana, Cuba
- ⁹ Centro de Investigación y de Estudios Avanzados (CINVESTAV), Mexico City and Mérida, Mexico
- ¹⁰ Centro Fermi - Museo Storico della Fisica e Centro Studi e Ricerche “Enrico Fermi”, Rome, Italy
- ¹¹ Chicago State University, Chicago, Illinois, United States
- ¹² China Institute of Atomic Energy, Beijing, China
- ¹³ Chonbuk National University, Jeonju, Republic of Korea
- ¹⁴ Comenius University Bratislava, Faculty of Mathematics, Physics and Informatics, Bratislava, Slovakia
- ¹⁵ COMSATS Institute of Information Technology (CIIT), Islamabad, Pakistan
- ¹⁶ Creighton University, Omaha, Nebraska, United States
- ¹⁷ Department of Physics, Aligarh Muslim University, Aligarh, India
- ¹⁸ Department of Physics, Pusan National University, Pusan, Republic of Korea
- ¹⁹ Department of Physics, Sejong University, Seoul, Republic of Korea
- ²⁰ Department of Physics, University of California, Berkeley, California, United States
- ²¹ Department of Physics, University of Oslo, Oslo, Norway
- ²² Department of Physics and Technology, University of Bergen, Bergen, Norway
- ²³ Dipartimento di Fisica dell’Università ‘La Sapienza’ and Sezione INFN, Rome, Italy
- ²⁴ Dipartimento di Fisica dell’Università and Sezione INFN, Cagliari, Italy
- ²⁵ Dipartimento di Fisica dell’Università and Sezione INFN, Trieste, Italy
- ²⁶ Dipartimento di Fisica dell’Università and Sezione INFN, Turin, Italy
- ²⁷ Dipartimento di Fisica e Astronomia dell’Università and Sezione INFN, Bologna, Italy
- ²⁸ Dipartimento di Fisica e Astronomia dell’Università and Sezione INFN, Catania, Italy
- ²⁹ Dipartimento di Fisica e Astronomia dell’Università and Sezione INFN, Padova, Italy
- ³⁰ Dipartimento di Fisica ‘E.R. Caianiello’ dell’Università and Gruppo Collegato INFN, Salerno, Italy
- ³¹ Dipartimento DISAT del Politecnico and Sezione INFN, Turin, Italy
- ³² Dipartimento di Scienze e Innovazione Tecnologica dell’Università del Piemonte Orientale and INFN Sezione di Torino, Alessandria, Italy
- ³³ Dipartimento Interateneo di Fisica ‘M. Merlin’ and Sezione INFN, Bari, Italy
- ³⁴ European Organization for Nuclear Research (CERN), Geneva, Switzerland
- ³⁵ Faculty of Electrical Engineering, Mechanical Engineering and Naval Architecture, University of Split, Split, Croatia
- ³⁶ Faculty of Engineering and Science, Western Norway University of Applied Sciences, Bergen, Norway
- ³⁷ Faculty of Nuclear Sciences and Physical Engineering, Czech Technical University in Prague, Prague, Czech Republic
- ³⁸ Faculty of Science, P.J. Šafárik University, Košice, Slovakia
- ³⁹ Frankfurt Institute for Advanced Studies, Johann Wolfgang Goethe-Universität Frankfurt, Frankfurt, Germany
- ⁴⁰ Gangneung-Wonju National University, Gangneung, Republic of Korea
- ⁴¹ Gauhati University, Department of Physics, Guwahati, India
- ⁴² Helmholtz-Institut für Strahlen- und Kernphysik, Rheinische Friedrich-Wilhelms-Universität Bonn, Bonn, Germany
- ⁴³ Helsinki Institute of Physics (HIP), Helsinki, Finland
- ⁴⁴ High Energy Physics Group, Universidad Autónoma de Puebla, Puebla, Mexico
- ⁴⁵ Hiroshima University, Hiroshima, Japan
- ⁴⁶ Hochschule Worms, Zentrum für Technologietransfer und Telekommunikation (ZTT), Worms, Germany
- ⁴⁷ Horia Hulubei National Institute of Physics and Nuclear Engineering, Bucharest, Romania
- ⁴⁸ Indian Institute of Technology Bombay (IIT), Mumbai, India
- ⁴⁹ Indian Institute of Technology Indore, Indore, India
- ⁵⁰ Indonesian Institute of Sciences, Jakarta, Indonesia
- ⁵¹ INFN, Laboratori Nazionali di Frascati, Frascati, Italy
- ⁵² INFN, Sezione di Bari, Bari, Italy
- ⁵³ INFN, Sezione di Bologna, Bologna, Italy
- ⁵⁴ INFN, Sezione di Cagliari, Cagliari, Italy
- ⁵⁵ INFN, Sezione di Catania, Catania, Italy
- ⁵⁶ INFN, Sezione di Padova, Padova, Italy
- ⁵⁷ INFN, Sezione di Roma, Rome, Italy
- ⁵⁸ INFN, Sezione di Torino, Turin, Italy

- 59 INFN, Sezione di Trieste, Trieste, Italy
- 60 Inha University, Incheon, Republic of Korea
- 61 Institut de Physique Nucléaire d'Orsay (IPNO), Institut National de Physique Nucléaire et de Physique des Particules (IN2P3/CNRS), Université de Paris-Sud, Université Paris-Saclay, Orsay, France
- 62 Institute for Nuclear Research, Academy of Sciences, Moscow, Russia
- 63 Institute for Subatomic Physics, Utrecht University/Nikhef, Utrecht, Netherlands
- 64 Institute for Theoretical and Experimental Physics, Moscow, Russia
- 65 Institute of Experimental Physics, Slovak Academy of Sciences, Košice, Slovakia
- 66 Institute of Physics, Homi Bhabha National Institute, Bhubaneswar, India
- 67 Institute of Physics of the Czech Academy of Sciences, Prague, Czech Republic
- 68 Institute of Space Science (ISS), Bucharest, Romania
- 69 Institut für Kernphysik, Johann Wolfgang Goethe-Universität Frankfurt, Frankfurt, Germany
- 70 Instituto de Ciencias Nucleares, Universidad Nacional Autónoma de México, Mexico City, Mexico
- 71 Instituto de Física, Universidade Federal do Rio Grande do Sul (UFRGS), Porto Alegre, Brazil
- 72 Instituto de Física, Universidad Nacional Autónoma de México, Mexico City, Mexico
- 73 iThemba LABS, National Research Foundation, Somerset West, South Africa
- 74 Johann-Wolfgang-Goethe Universität Frankfurt Institut für Informatik, Fachbereich Informatik und Mathematik, Frankfurt, Germany
- 75 Joint Institute for Nuclear Research (JINR), Dubna, Russia
- 76 Korea Institute of Science and Technology Information, Daejeon, Republic of Korea
- 77 KTO Karatay University, Konya, Turkey
- 78 Laboratoire de Physique Subatomique et de Cosmologie, Université Grenoble-Alpes, CNRS-IN2P3, Grenoble, France
- 79 Lawrence Berkeley National Laboratory, Berkeley, California, United States
- 80 Lund University Department of Physics, Division of Particle Physics, Lund, Sweden
- 81 Nagasaki Institute of Applied Science, Nagasaki, Japan
- 82 Nara Women's University (NWU), Nara, Japan
- 83 National and Kapodistrian University of Athens, School of Science, Department of Physics, Athens, Greece
- 84 National Centre for Nuclear Research, Warsaw, Poland
- 85 National Institute of Science Education and Research, Homi Bhabha National Institute, Jatni, India
- 86 National Nuclear Research Center, Baku, Azerbaijan
- 87 National Research Centre Kurchatov Institute, Moscow, Russia
- 88 Niels Bohr Institute, University of Copenhagen, Copenhagen, Denmark
- 89 Nikhef, National institute for subatomic physics, Amsterdam, Netherlands
- 90 NRC Kurchatov Institute IHEP, Protvino, Russia
- 91 NRNU Moscow Engineering Physics Institute, Moscow, Russia
- 92 Nuclear Physics Group, STFC Daresbury Laboratory, Daresbury, United Kingdom
- 93 Nuclear Physics Institute of the Czech Academy of Sciences, Řež u Prahy, Czech Republic
- 94 Oak Ridge National Laboratory, Oak Ridge, Tennessee, United States
- 95 Ohio State University, Columbus, Ohio, United States
- 96 Petersburg Nuclear Physics Institute, Gatchina, Russia
- 97 Physics department, Faculty of science, University of Zagreb, Zagreb, Croatia
- 98 Physics Department, Panjab University, Chandigarh, India
- 99 Physics Department, University of Jammu, Jammu, India
- 100 Physics Department, University of Rajasthan, Jaipur, India
- 101 Physikalisches Institut, Eberhard-Karls-Universität Tübingen, Tübingen, Germany
- 102 Physikalisches Institut, Ruprecht-Karls-Universität Heidelberg, Heidelberg, Germany
- 103 Physik Department, Technische Universität München, Munich, Germany
- 104 Research Division and ExtreMe Matter Institute EMMI, GSI Helmholtzzentrum für Schwerionenforschung GmbH, Darmstadt, Germany
- 105 Rudjer Bošković Institute, Zagreb, Croatia
- 106 Russian Federal Nuclear Center (VNIIEF), Sarov, Russia
- 107 Saha Institute of Nuclear Physics, Homi Bhabha National Institute, Kolkata, India
- 108 School of Physics and Astronomy, University of Birmingham, Birmingham, United Kingdom
- 109 Sección Física, Departamento de Ciencias, Pontificia Universidad Católica del Perú, Lima, Peru

- 110 Shanghai Institute of Applied Physics, Shanghai, China
- 111 St. Petersburg State University, St. Petersburg, Russia
- 112 Stefan Meyer Institut für Subatomare Physik (SMI), Vienna, Austria
- 113 SUBATECH, IMT Atlantique, Université de Nantes, CNRS-IN2P3, Nantes, France
- 114 Suranaree University of Technology, Nakhon Ratchasima, Thailand
- 115 Technical University of Košice, Košice, Slovakia
- 116 Technische Universität München, Excellence Cluster 'Universe', Munich, Germany
- 117 The Henryk Niewodniczanski Institute of Nuclear Physics, Polish Academy of Sciences, Cracow, Poland
- 118 The University of Texas at Austin, Austin, Texas, United States
- 119 Universidad Autónoma de Sinaloa, Culiacán, Mexico
- 120 Universidade de São Paulo (USP), São Paulo, Brazil
- 121 Universidade Estadual de Campinas (UNICAMP), Campinas, Brazil
- 122 Universidade Federal do ABC, Santo Andre, Brazil
- 123 University College of Southeast Norway, Tonsberg, Norway
- 124 University of Cape Town, Cape Town, South Africa
- 125 University of Houston, Houston, Texas, United States
- 126 University of Jyväskylä, Jyväskylä, Finland
- 127 University of Liverpool, Liverpool, United Kingdom
- 128 University of Science and Technology of China, Hefei, China
- 129 University of Tennessee, Knoxville, Tennessee, United States
- 130 University of the Witwatersrand, Johannesburg, South Africa
- 131 University of Tokyo, Tokyo, Japan
- 132 University of Tsukuba, Tsukuba, Japan
- 133 Université Clermont Auvergne, CNRS/IN2P3, LPC, Clermont-Ferrand, France
- 134 Université de Lyon, Université Lyon 1, CNRS/IN2P3, IPN-Lyon, Villeurbanne, Lyon, France
- 135 Université de Strasbourg, CNRS, IPHC UMR 7178, F-67000 Strasbourg, France, Strasbourg, France
- 136 Université Paris-Saclay Centre d'Études de Saclay (CEA), IRFU, Department de Physique Nucléaire (DPhN), Saclay, France
- 137 Università degli Studi di Foggia, Foggia, Italy
- 138 Università degli Studi di Pavia, Pavia, Italy
- 139 Università di Brescia, Brescia, Italy
- 140 Variable Energy Cyclotron Centre, Homi Bhabha National Institute, Kolkata, India
- 141 Warsaw University of Technology, Warsaw, Poland
- 142 Wayne State University, Detroit, Michigan, United States
- 143 Westfälische Wilhelms-Universität Münster, Institut für Kernphysik, Münster, Germany
- 144 Wigner Research Centre for Physics, Hungarian Academy of Sciences, Budapest, Hungary
- 145 Yale University, New Haven, Connecticut, United States
- 146 Yonsei University, Seoul, Republic of Korea